

# Carbon isotopes in the ocean model of the Community Earth System Model (CESM1)

Alexandra Jahn<sup>1\*</sup>, Keith Lindsay<sup>1</sup>, Xavier Giraud<sup>2,3</sup>, Nicolas Gruber<sup>3</sup>, Bette L. Otto-Bliesner<sup>1</sup>, Zhengyu Liu<sup>4</sup>, and Esther C. Brady<sup>1</sup>

<sup>1</sup>National Center for Atmospheric Research, Climate and Global Dynamics Division, Boulder, CO, USA

<sup>2</sup>Aix Marseille Université, CNRS, IRD, Collège de France, CEREGE UM34, Aix en Provence, France

<sup>3</sup>Environmental Physics Group, Institute of Biogeochemistry and Pollutant Dynamics, ETH Zürich, Zürich, Switzerland

<sup>4</sup>Department of Atmospheric and Oceanic Sciences, and Center for Climatic Research, University of Wisconsin – Madison, Madison, WI, USA

\*Now at the Department of Atmospheric and Oceanic Sciences and the Institute of Arctic and Alpine Research at the University of Colorado Boulder, Boulder, CO, USA

*Correspondence to:* Alexandra Jahn  
(alexandra.jahn@colorado.edu)

## Abstract.

Carbon isotopes in the ocean are frequently used as paleo climate proxies and as present-day geochemical ocean tracers. In order to allow a more direct comparison of climate model results with this large and currently underutilized dataset, we added a carbon isotope module to the ocean model of the Community Earth System Model (CESM), containing the cycling of the stable isotope <sup>13</sup>C and the radioactive isotope <sup>14</sup>C. We implemented the <sup>14</sup>C tracer in two ways: in the “abiotic” case, the <sup>14</sup>C tracer is only subject to air–sea gas exchange, physical transport, and radioactive decay, while in the “biotic” version, the <sup>14</sup>C additionally follows the <sup>13</sup>C tracer through all biogeochemical and ecological processes. Thus, the abiotic <sup>14</sup>C tracer can be run without the ecosystem module, requiring significantly less computational resources. The carbon isotope module calculates the carbon isotopic fractionation during gas exchange, photosynthesis, and calcium carbonate formation, while any subsequent biological process such as remineralization as well as any external inputs are assumed to occur without fractionation. Given the uncertainty associated with the biological fractionation during photosynthesis, we implemented and tested three parameterizations of different complexity. Compared to present-day observations, the model is able to simulate the oceanic <sup>14</sup>C bomb uptake and the <sup>13</sup>C Suess effect reasonably well compared to observations and other model studies. At the same time, the carbon isotopes reveal biases in the physical model, for example a too sluggish ventilation of the deep Pacific Ocean.

## 1 Introduction

20 A large fraction of paleoclimatic reconstructions are based on isotopic measurements (e.g. Petit et al.,  
1999; McDermott, 2004; Curry and Oppo, 2005; Polka et al., 2013), yet there are many uncertainties  
associated with the interpretation of these records in terms of physical climate variables such as  
temperature, precipitation, and ocean circulation rates. More direct comparisons of paleo data with  
climate models would therefore be beneficial, both to test the interpretation of the isotopic proxy  
25 data and to allow for better comparisons of model simulations with proxy data. Furthermore, many  
isotope tracers are currently being measured in the ocean, and including them in ocean models can  
help us better understand the ocean circulation and diagnose model biases (e.g. Matsumoto et al.,  
2004). For all of these reasons, we have added a carbon isotope module to the ocean model of the  
Community Earth System Model (CESM) (Hurrell et al., 2013).

30 Carbon has two stable isotopes,  $^{12}\text{C}$  and  $^{13}\text{C}$ . More than 98.9% of carbon on earth is  $^{12}\text{C}$ ,  
while  $^{13}\text{C}$  makes up most of the remaining 1%. The radioactive carbon isotope  $^{14}\text{C}$ , also called  
radiocarbon, is present only in trace amounts (approximately  $1 \times 10^{-10}\%$  of all carbon) and has  
a half-life of 5730 years (Godwin, 1962). Radiocarbon is a useful tracer to evaluate the ventilation  
of the deep ocean because it acts as a clock, measuring the time since water was last in contact with  
35 the atmosphere (e.g. Toggweiler et al., 1989; Orr, 2002; Meissner et al., 2003; Waugh et al., 2003;  
Key et al., 2004; Doney et al., 2004; Matsumoto et al., 2004; Meissner, 2007; Bardin et al., 2014).  
Because of the atmospheric nuclear weapons tests in the 1950s and 1960s and the well-known input-  
function of radiocarbon during this time, radiocarbon is also useful to evaluate the recent penetration  
of anthropogenic carbon into the ocean (e.g. Graven et al., 2012). Furthermore, oceanic radiocarbon  
40 has been used to determine the mean gas exchange velocity used in ocean models (e.g. Wanninkhof,  
1992; Sweeney et al., 2007; Naegler et al., 2006; Naegler, 2009). Oceanic  $\delta^{13}\text{C}$  has been used in  
paleoclimate studies as a tracer of the ocean circulation (e.g. Marchal et al., 1998; Curry and Oppo,  
2005; Crucifix, 2005), to calculate the uptake of anthropogenic carbon dioxide (e.g. Keeling et al.,  
1980; Quay et al., 1992; Gruber et al., 1999; Sonnerup et al., 1999; Gruber and Keeling, 2001), and  
45 to diagnose biases in marine ecosystem models (e.g. Schmittner et al., 2013).

We added the carbon isotopes to the code so that they follow the cycling of total carbon through  
all ecosystem and physical/chemical processes. In this biotic formulation, a new  $^{13}\text{C}$  and  $^{14}\text{C}$  state  
variable was added to each carbon-bearing state variable resulting in a total of 14 new state variables.  
For  $^{14}\text{C}$ , we also added the option of a simplified representation, where the isotope is only subject to  
50 the main chemical and physical processes during gas exchange and decay, but does not cycle through  
the ecosystem. This abiotic formulation of  $^{14}\text{C}$  was implemented based on the Ocean Carbon Model  
Intercomparison Project Phase 2 (OCMIP-2) protocol (Orr et al., 2000).

Abiotic radiocarbon had been added previously to the NCAR ocean model (in NCOM1.4, Orr,  
2002, and POP1/CCSM3, Graven et al., 2012), and biotic  $^{13}\text{C}$  was implemented into the ecosystem  
55 model of the CCSM3 by X. Giraud and N. Gruber in 2009–2010. However, neither development was

ever added to the trunk of the ocean model code of the CESM, so it was not maintained as the model evolved over the years and consequently none of these implementations still work in the current ocean model of the CESM. In contrast, the addition of a biotic radiocarbon tracer is completely new in this implementation in the CESM. In order to increase the chances of maintaining these  
60 developments as the model continues to evolve, the current implementation has been added to the code trunk of the current ocean model of CESM. By including carbon isotopes in the ocean model of the CESM1, the CESM1 joins the community of other comprehensive ocean general circulation models that include abiotic radiocarbon and/or biotic  $^{13}\text{C}$  in the ocean (e.g. MoBidiC, Crucifix, 2005, PISCES, Tagliabue and Bopp, 2008, CM2Mc ESM, Galbraith et al., 2011, HAMOCC2s,  
65 Hesse et al., 2011, and UVic ESCM, e.g. Meissner et al., 2003; Schmittner et al., 2013). While the abiotic radiocarbon implementation tends to follow the OCMIP-2 protocol (Orr et al., 2000) in all models, the implementations of biotic  $^{13}\text{C}$  differs between models, mainly due to the complexity of the ocean biogeochemistry model used in them, but also due to different choices in regards to the parameterization of the biological fractionation during photosynthesis and calcium carbonate  
70 formation.

As a reference for future studies using these new capabilities in the CESM, we describe the model used (Sect. 2), describe the details of the implementation of the abiotic and biotic carbon isotopes (Sect. 3), and compare the simulated carbon isotope fields to observational data to show the general performance of the model (Sect. 4).

## 75 **2 Model**

This work was done using the code base of the Community Earth System Model (CESM) (Hurrell et al., 2013), version 1.0.5. The isotope code has been updated to the current version of the CESM and is targeted for public release in 2016 as part of CESM2 (see the section on code availability at the end of the article). The CESM is a fully-coupled climate model with components for the  
80 atmosphere, land, river runoff, sea ice, ocean and ice sheets, coupled by a coupler. Its components and simulations have been described in a large collection of articles, many of them contained in a special collection in the Journal of Climate (<http://journals.ametsoc.org/page/CCSM4/CESM1>). The simulations analyzed here were performed using the ocean model coupled to data models for the atmosphere, the land, the sea ice, and the river routing, using repeated normal year forcing from  
85 CORE-II (Large and Yeager, 2009). The ocean model was run at a nominal  $3^\circ$  horizontal resolution with 60 vertical levels, which is the low-resolution configuration of the ocean model (Shields et al., 2012). This ocean-only model version with ocean biogeochemistry at  $3^\circ$  model resolution is used as a low-cost testbed for model development, but is not scientifically validated or supported. Hence, future science applications should use the fully-coupled  $1^\circ$  horizontal resolution model version of  
90 the CESM.

### 3 Carbon isotope implementation

The carbon isotopes were added as optional passive tracers, with the biotic and abiotic implementations as two different options that can be set at the compilation and build time. The abiotic  $^{14}\text{C}$  can be run with or without the ocean ecosystem model, while the biotic  $^{13}\text{C}$  and  $^{14}\text{C}$  require the ocean ecosystem model to be turned on.

#### 3.1 Abiotic $^{14}\text{C}$

In this implementation,  $\text{DI}^{14}\text{C}$  is the model's normalized concentration of total dissolved inorganic  $^{14}\text{C}$ , following the OCMIP2 protocol (Orr et al., 2000).  $\text{DI}^{14}\text{C}$  is used as normalized concentration in order to minimize the numerical error of carrying very small numbers. The normalization is done by dividing the real  $\text{DI}^{14}\text{C}$  by the standard ratio of  $^{14}\text{C}/^{12}\text{C}=1.176 \times 10^{-12}$  (Karlen et al., 1968). To obtain comparable  $\text{DI}^{14}\text{C}$  values as measured, we multiply the simulated  $\text{DI}^{14}\text{C}$  by this scaling factor of  $1.176 \times 10^{-12}$ . Since the abiotic radiocarbon is designed to be run without the ocean ecosystem active, we also carry an abiotic  $\text{DI}^{12}\text{C}$  tracer to calculate the isotope ratio  $^{14}R = \text{DI}^{14}\text{C}/\text{DI}^{12}\text{C}$ . For comparisons with observations, we calculate  $\Delta^{14}\text{C}$  as a diagnostic variable:

$$\Delta^{14}\text{C}=(^{14}R-1) \cdot 1000. \quad (1)$$

By construction, the abiotic  $\text{DI}^{12}\text{C}$  and  $\text{DI}^{14}\text{C}$  tracers only depend on the solubility of carbon in seawater and neglect all biological activity. The error in  $\Delta^{14}\text{C}$  due to neglecting biology activity has been estimated to be on the order of 10 % (Fiadiero, 1982).

Note that we do not multiply  $^{14}R$  by  $^{14}R_{\text{std}}$  in Eq. (1), as we are using a normalized  $\text{DI}^{14}\text{C}$  (following Orr et al., 2000). Given that this abiotic implementation does not account for the fractionation during gas exchange, we do not apply the correction for fractionation that is commonly applied to observational measurements of  $^{14}\text{C}/^{12}\text{C}$  ratios (as well as for the biotic  $^{14}\text{C}$  implementation, see Eq. (27) in Sect. 3.2.4). The simulated abiotic  $\Delta^{14}\text{C}$  is therefore directly comparable to observed data reported as  $\Delta^{14}\text{C}$  (see Toggweiler et al., 1989, for more details).

#### 3.1.1 Surface fluxes

We follow the abiotic OCMIP-2 protocol (Orr et al., 2000) for most of the implementation of the abiotic radiocarbon surface fluxes, with the following notable differences:

- We use a coefficient  $a$  of  $0.31 \text{ cm h}^{-1}$  (Wanninkhof, 1992) instead of  $0.337 \text{ cm h}^{-1}$  as used in OCMIP-2. This is higher than what most recent estimates suggest (e.g., Sweeney et al., 2007; Naegler et al., 2006; Naegler, 2009; Graven et al., 2012), but makes it consistent with the gas-transfer formulation used in other parts of the CESM.
- We use the daily mean of the squared 10 m windspeed (either from the prescribed CORE-II forcing or from the coupled atmospheric model) instead of the climatology of the squared

125 monthly average of the instantaneous SSMI velocity and its instantaneous variance as used in OCMIP-2.

- We use the daily mean of the ice fraction and atmospheric pressure (either from the data models or the coupled sea ice and atmosphere models) instead of the monthly averaged climatology used in OCMIP-2.
- We use a constant reference value ( $1944 \mu\text{mol m}^{-3}$ ) for the virtual fluxes of abiotic radiocarbon, rather than an annually updated average of the surface  $\text{DI}^{14}\text{C}$  as suggested in OCMIP-2. This is done to conserve total  $^{14}\text{C}$  in the model (in absence of radioactive decay).

130 To compute the partial pressure of  $\text{CO}_2$  from the abiotic  $\text{DI}^{12}\text{C}$ , we require an estimate of surface alkalinity. We follow again OCMIP-2, i.e., we estimate surface alkalinity (Alk) by scaling the ocean mean alkalinity,  $\text{Alkbar} = 2310 \text{ microeq kg}^{-1}$  with sea-surface salinity, SSS, i.e.,

$$135 \text{ Alk} = \text{Alkbar} \cdot \rho_{\text{sw}} \cdot \text{SSS} / S_{\text{Ref}} \quad (2)$$

with  $S_{\text{Ref}} = 34.7$  and  $\rho_{\text{sw}} = 4.1/3.996 \text{ g cm}^{-3}$  (these two are constants in the CESM). We alter this calculation in the Baltic Sea and the Black Sea to avoid unrealistic Alkalinity values, following the procedure developed by K. Lindsay for creating initial conditions for the marine ecosystem model: in the Black Sea, the surface alkalinity is independent of SSS:  $\text{alkalinity} = 3300 \cdot \rho_{\text{sw}}$ . In the Baltic Sea, we calculate Alkalinity depending on the surface salinity, with  $\text{Alkalinity} = 119 + 196 \cdot \text{SSS}$  when SSS is equal to or below 7.3, and  $\text{Alkalinity} = 1237 + 43 \cdot \text{SSS}$  when the SSS is above 7.3. The computation of  $p\text{CO}_2$  also requires an assumption about the surface ocean concentrations of silicic acid and phosphate, for which we use OCMIP-2's global constants, i.e.,  $7.5 \mu\text{mol kg}^{-1}$  for silicic acid,  $\text{Si}(\text{OH})_4$ , and  $0.5 \mu\text{mol kg}^{-1}$  for phosphate,  $\text{PO}_4$ .

#### 145 **Air–sea gas exchange**

As in OCMIP-2, the air–sea gas exchange flux of  $^{12}\text{C}$  is calculated as

$$F = \text{PV} \cdot (C_{\text{sat}} - C_{\text{surf}}) \quad (3)$$

with PV being the  $\text{CO}_2$  gas transfer velocity (called the piston velocity) in  $\text{ms}^{-1}$ , calculated as

$$\text{PV} = (1 - \text{aice}) \cdot a \cdot u_{10}^2 \cdot (660.0 / Sc_{\text{CO}_2})^{-1/2}. \quad (4)$$

150 The coefficient  $a$  is taken as  $0.31 \text{ cm h}^{-1}$  as mentioned earlier, aice is the fraction of the ocean covered by sea ice,  $u_{10}^2$  is the squared 10 m wind speed from the coupler, and  $Sc_{\text{CO}_2}$  is the Schmidt number of  $\text{CO}_2$ .  $Sc_{\text{CO}_2}$  is calculated as in the ecosystem model, following Wanninkhof (1992):

$$Sc_{\text{CO}_2} = 2073.1 + \text{SST} \cdot (-125.62 + \text{SST} \cdot (3.6276 + \text{SST} \cdot (-0.043219))). \quad (5)$$

$C_{\text{surf}}$  in the gas flux calculation above is the surface aqueous  $\text{CO}_2$  concentration in  $\text{mol m}^{-3}$  (also  
 155 called  $\text{CO}_2^*$ , which is the aqueous  $\text{CO}_2$  concentration in  $\text{mol m}^{-3}$  in the ocean in general).  $C_{\text{sat}}$  is  
 the saturation concentration in  $\text{mol m}^{-3}$ , with  $C_{\text{sat}} = \text{CO}_2^* + \text{DCO}_2^*$  and  $\text{DCO}_2^*$  being the difference  
 in  $\text{CO}_2$  concentration between the surface ocean and the atmosphere. SST is the sea surface tem-  
 perature.  $\text{CO}_2^*$  and  $\text{DCO}_2^*$  in turn are calculated by the carbonate solver from the ecosystem model,  
 based on SST, SSS, ALK,  $\text{PO}_4$ ,  $\text{Si}(\text{OH})_4$ , pH, atmospheric  $p\text{CO}_2$ , atmospheric pressure, and the  
 160 abiotic  $\text{DI}^{12}\text{C}$  and  $\text{DI}^{14}\text{C}$  concentration in the surface water.

As in OCMIP-2, we do not account for fractionation during gas exchange in this abiotic formu-  
 lation, as the effect of isotopic fractionation is almost completely accounted for by the standard  
 correction made when calculating  $\Delta^{14}\text{C}$  from observations (see Toggweiler et al., 1989, for details).

The gas flux of the normalized abiotic  $\text{DI}^{14}\text{C}$  is calculated as

$$165 \quad F^{14} = PV \cdot (C_{\text{sat}} \cdot R^{14}\text{C}_{\text{atm}} - C_{\text{surf}} \cdot R^{14}\text{C}_{\text{ocn}}) \quad (6)$$

with

$$R^{14}\text{C}_{\text{atm}} = (1 + \Delta^{14}\text{C}_{\text{atm}}/1000) \quad (7)$$

and

$$R^{14}\text{C}_{\text{ocn}} = 1000 \cdot (\text{DI}^{14}\text{C}/\text{DI}^{12}\text{C} - 1). \quad (8)$$

170 The values of the atmospheric  $p\text{CO}_2$  and  $\Delta^{14}\text{C}_{\text{atm}}$  can be set to be constants or can be read in from  
 a file. For atmospheric  $p\text{CO}_2$ , it can also be taken from the coupler, to ensure the use of a consistent  
 atmospheric  $p\text{CO}_2$  value across model components. Currently the code is set up to read in three files  
 of  $\Delta^{14}\text{C}_{\text{atm}}$  values, one each for the Northern Hemisphere, the equatorial region ( $20^\circ \text{N}$ – $20^\circ \text{S}$ ), and  
 the Southern Hemisphere, in order to represent the spatial inhomogeneity of  $\Delta^{14}\text{C}_{\text{atm}}$ , for example  
 175 after the atmospheric nuclear bomb tests.

### Virtual fluxes

The CESM ocean model is a volume-conserving model where water fluxes at the surface (from  
 precipitation, evaporation, and river input) are added as virtual fluxes. These virtual fluxes represent  
 the dilution or concentration effect from adding or removing freshwater. For the abiotic carbon  
 180 isotope tracers, we have a virtual  $\text{DI}^{12}\text{C}$  and  $\text{DI}^{14}\text{C}$  flux. As for salinity and for DIC in the ecosystem  
 model, we use a constant surface reference  $\text{DI}^{12}\text{C}$  and  $\text{DI}^{14}\text{C}$  for the calculation of virtual fluxes in  
 order to conserve tracers. The reference values are  $1944 \mu\text{mol m}^{-3}$  for both  $\text{DI}^{12}\text{C}$  and normalized  
 $\text{DI}^{14}\text{C}$ , the same as for DIC in the ecosystem model of CESM.

### 3.1.2 Interior processes

185 In the interior of the ocean, the only additional term to the transport of the tracers by the physical ocean model is the decay term for  $\text{DI}^{14}\text{C}$ , following the OCMIP-2 protocol.

$$d[\text{DI}^{12}\text{C}]/dt=L([\text{DI}^{12}\text{C}]) \quad (9)$$

and

$$d[\text{DI}^{14}\text{C}]/dt=L([\text{DI}^{14}\text{C}])-\lambda \cdot [\text{DI}^{14}\text{C}] \quad (10)$$

190 with  $L$  being the 3-D transport operator and  $\lambda$  being the radioactive decay constant for  $^{14}\text{C}$  in  $\text{s}^{-1}$ , using a half-life of 5730 years (Godwin, 1962):

$$\lambda = \ln(2)/(5730 \cdot 31556926). \quad (11)$$

The radiocarbon age (relative to AD 1950 = 0 yr BP) is calculated from  $\Delta^{14}\text{C}$  following:

$$^{14}\text{C}_{\text{age}} = -5730/\ln 2 \times \ln(1 + \Delta^{14}\text{C}/1000) \quad (12)$$

195 5730 years /  $\ln 2 = 8267$  years is the mean life of  $^{14}\text{C}$ , which differs from the often used mean-life of 8033 years (e.g. Stuiver and Polach, 1977), which is based on the earlier Libby half-life of 5568 (Libby, 1955).

### 3.2 Biotic $^{13}\text{C}$ and $^{14}\text{C}$

In the biotic implementation of  $^{13}\text{C}$  and  $^{14}\text{C}$ , we use the ocean ecosystem model (e.g. Moore et al.,  
200 2013) to compute the carbon pools as well as all other biological variables (like silicic acid, alkalinity, etc). The ecosystem model currently has seven carbon pools: DIC, DOC (dissolved organic carbon),  $\text{CaCO}_3$ , diazotrophs, diatoms, small phytoplankton, and zooplankton. We carry passive tracers for each of these in the isotope-enabled version of the code. As  $^{12}\text{C}$  makes up over 98 % of the carbon earth and does not fractionate, we assume that the ecosystem carries  $^{12}\text{C}$ . This means that  
205 the isotope ratio  $R$  can be calculated as the ratio of the new isotopic carbon pools to the ecosystem carbon pools. As for the abiotic radiocarbon, we use scaled variables for  $^{13}\text{C}$  and  $^{14}\text{C}$  in order to minimize the numerical error of carrying very small numbers (particularly for  $^{14}\text{C}$ ). The scaling factor is the commonly used standard  $^{13}\text{C}/^{12}\text{C}$  for each isotope, i.e.,  $1.12372 \times 10^{-8}$  for  $\text{iso} = ^{13}\text{C}$  (Craig, 1957) and  $1.176 \times 10^{-12}$  for  $\text{iso} = ^{14}\text{C}$  (Karlen et al., 1968). This means that we use  $^{13}R_{\text{Std}} = 1$   
210 and  $^{14}R_{\text{Std}} = 1$  in the code, and that the model simulated isotopic carbon pools are multiplied by the respective scaling factor to compare them with observations.

In the biotic formulation, we account for the fractionation of  $^{13}\text{C}$  and  $^{14}\text{C}$  during gas exchange and during biological processes. The fractionation ( $\epsilon$ ) of  $^{14}\text{C}$  is always twice that of  $^{13}\text{C}$ , as all relevant processes have a mass-dependent fractionation for carbon (Bigeleisen, 1952; Craig, 1954).

215 The isotopic fractionation  $\epsilon$  is related to the fractionation factor  $\alpha$  through:

$$\epsilon = (\alpha - 1) \cdot 1000. \quad (13)$$

As diagnostic variable, we compute the  $\delta^{\text{iso}}\text{C}$  values by first computing the ratio  $^{\text{iso}}R = \text{DI}^{\text{iso}}\text{C}/\text{DIC}$ , and then using

$$\delta^{\text{iso}}\text{C} = (^{\text{iso}}R - 1) \cdot 1000. \quad (14)$$

220 As for the abiotic  $\Delta^{14}\text{C}$  calculation in Eq. (1), we do not multiply by  $^{\text{iso}}R_{\text{Std}}$  in the calculation of  $\delta^{\text{iso}}\text{C}$  because we are using normalized  $\text{DI}^{\text{iso}}\text{C}$ .

### 3.2.1 Air-sea gas exchange of $^{13}\text{C}$

The air-sea flux of  $^{13}\text{C}$  is calculated based on Zhang et al. (1995):

$$F^{13} = PV \cdot \alpha_{\text{aq}_g} \cdot \alpha_k \cdot (R^{13}\text{C}_{\text{atm}} \cdot C_{\text{sat}} - R^{13}\text{C}_{\text{DIC}} \cdot C_{\text{surf}} / \alpha_{\text{DIC}_g}). \quad (15)$$

225 Here,  $C_{\text{sat}}$  and  $C_{\text{surf}}$  are obtained from the ecosystem model.  $\alpha_k = -0.99919$  is the constant kinetic fractionation factor from Zhang et al. (1995) (with  $\epsilon = -0.81$  and  $\alpha = \epsilon/1000 + 1$ ).  $\alpha_{\text{aq}_g}$  is the temperature (TEMP, in  $^{\circ}\text{C}$ ) dependent isotopic fractionation factor during gas dissolution, based on the equation for  $\epsilon_{\text{aq}_g}$  from Zhang et al. (1995).

$$\epsilon_{\text{aq}_g} = -0.0049 \cdot \text{TEMP} - 1.31. \quad (16)$$

230 The temperature and carbonate fraction ( $f_{\text{CO}_3}$ ) dependent fractionation factor ( $\alpha_{\text{DIC}_g}$ ) between total DIC and  $\text{CO}_2$  is based on the empirical relationship for  $\epsilon_{\text{DIC}_g}$  from Zhang et al. (1995):

$$\epsilon_{\text{DIC}_g} = 0.014 \cdot \text{TEMP} \cdot f_{\text{CO}_3} - 0.105 \cdot \text{TEMP} + 10.53. \quad (17)$$

$R^{13}\text{C}_{\text{atm}}$  is the  $^{13}\text{C}$  to  $^{12}\text{C}$  ratio in atmospheric  $\text{CO}_2$ , calculated using the atmospheric  $\delta^{13}\text{C}_{\text{atm}}$  record and  $R_{\text{atm}} = 1 + \delta^{13}\text{C}_{\text{atm}}/1000$  (scaled by  $^{13}R_{\text{Std}}$ ). The values of  $\delta^{13}\text{C}_{\text{atm}}$  can be set to be  
235 a constant or it can be read in from a file. Currently  $\delta^{13}\text{C}_{\text{atm}}$  is assumed to be well mixed globally, so only one global value is read in. With small code modifications globally inhomogeneous  $\delta^{13}\text{C}_{\text{atm}}$  values can easily be read in instead.  $R^{13}\text{C}_{\text{DIC}}$  is the  $^{13}\text{C}$  to  $^{12}\text{C}$  ratio of dissolved inorganic carbon, calculated from the simulated biotic DIC and  $\text{DI}^{13}\text{C}$ .

### 3.2.2 Virtual fluxes of $^{13}\text{C}$

240 As stated in Sect. 3.1.1, we account for the dilution and concentration effect of surface freshwater fluxes in the model by adding a virtual flux, using a constant surface reference  $\text{DI}^{13}\text{C}$  (and  $\text{DI}^{14}\text{C}$ ) of  $1944 \mu\text{mol m}^{-3}$  for the calculation of virtual fluxes.

### 3.2.3 Biological fractionation of $^{13}\text{C}$

The isotopic carbon-fixation by photosynthesis (photo $^{13}\text{C}$ ) is computed from the  $^{12}\text{C}$  fixation during  
 245 photosynthesis (photoC, from the ecosystem model), using

$$\text{photo}^{13}\text{C} = \text{photoC} \cdot R_p \quad (18)$$

with

$$R_p = 1000 \cdot R_{\text{CO}_2^*} / (\epsilon_p + 1000) \quad (19)$$

and

$$250 \quad R_{\text{CO}_2^*} = R^{13}\text{C}_{\text{DIC}} \cdot \alpha_{\text{aq}_g} / \alpha_{\text{DIC}_g}. \quad (20)$$

The strength of the biological fractionation of carbon during photosynthesis ( $\epsilon_p$ ), as well as the  
 key controlling parameters, are still being debated in the literature (e.g. Keller and Morel, 1999), and  
 many of the existing  $^{13}\text{C}$  implementations in models use different parameterizations. We therefore  
 implemented three different parameterizations for  $\epsilon_p$  to test the sensitivity of our results to the choice  
 255 of biological fractionation.

The simplest model for  $\epsilon_p$  by Rau et al. (1989) gives the same  $\epsilon_p$  value for all types of autotrophs:

$$\epsilon_p = 1000 \cdot (\delta_{\text{CO}_2^*} - \delta_{\text{C}_p}) / (1000 + \delta_{\text{C}_p}). \quad (21)$$

This relationship is based on the empirical relationship found by Rau et al. (1989) between the  
 isotopic composition of the autotroph ( $\delta_{\text{C}_p}$ ) and  $\text{CO}_2^*$ :

$$260 \quad \delta_{\text{C}_p} = -0.8 \cdot \text{CO}_2^* - 12.6, \quad (22)$$

limiting  $\delta_{\text{C}_p}$  to values between  $-18$  and  $-32\text{‰}$  (Rau et al., 1989).

Laws et al. (1995) assumed that  $\text{CO}_2$  enters the cell by diffusion and that the fractionation depends  
 on the rate of photosynthesis, and therefore parameterized  $\epsilon_p$  as a function of  $\text{CO}_2^*$  and the specific  
 photosynthesis rate of each phytoplankton group ( $\mu$ , in  $\text{s}^{-1}$ , calculated by the ecosystem model):

$$265 \quad {}^{13}\epsilon_p = (\mu / \text{CO}_2^* \cdot 86400 - 0.371) / (-0.015). \quad (23)$$

Keller and Morel (1999) argued that only considering diffusive  $\text{CO}_2$  transport into cells and as-  
 suming a linear relationship between  $\epsilon_p$  and  $\text{CO}_2^*$  concentration and the specific growth rate ( $\mu$ ) does  
 not agree with laboratory and field data, citing work by Sikes et al. (1980), Tortell et al. (1997), and  
 Laws et al. (1997). Keller and Morel (1999) therefore proposed to use phytoplankton-type specific  
 270 (constant) cell parameters (see Table 1) to compute the fractionation during photosynthesis:

$${}^{13}\epsilon_p = \epsilon_{\text{diff}} + (C_{\text{up}} / (C_{\text{up}} + 1/\text{var})) \cdot \delta_{\text{d}^{13}\text{C}} + \theta \cdot (\epsilon_{\text{fix}} - \epsilon_{\text{diff}}) \quad (24)$$

where

$$\theta = (1 + (C_{\text{up}} - 1) \cdot \text{var}) / (1 + C_{\text{up}} \cdot \text{var}) \quad (25)$$

and

$$\text{var} = \mu / \text{CO}_2^* \cdot 1000 \cdot \text{Qc} / (\text{cell}_{\text{permea}} \cdot \text{cell}_{\text{surf}}) \quad (26)$$

with Qc being the cell carbon content,  $\text{cell}_{\text{permea}}$  being the cell wall permeability to  $\text{CO}_2$  (aq),  $\text{cell}_{\text{surf}}$  being the surface areas of cells,  $C_{\text{up}}$  being the ratio of active carbon uptake to carbon fixation,  $\epsilon_{\text{fix}}$  being a constant phytoplankton-type dependent fractionation effect of carbon fixation,  $\epsilon_{\text{diff}} = 0.7$  representing the fractionation by diffusion (O'Leary, 1984), and  $\delta_{\text{d13C}} = -9.0$  being the difference  
 280 between the isotopic compositions of the external  $\text{CO}_2$  and the organic matter pools (Goericke et al., 1994).

While the fractionation during calcium carbonate formation is much smaller than the fractionation during photosynthesis (Turner, 1982), we include a small constant fractionation of 2‰ for calcium carbonate formation, based on work by Ziveri et al. (2003) that found a range of 3‰ to -2‰ for different species. Other implementations of  $^{13}\text{C}$  in ocean models have used values of 1‰ (e.g. Sonnerup et al., 1999; Tagliabue and Bopp, 2008) or have assumed no isotopic fractionation for calcification (e.g. Marchal et al., 1998; Schmittner et al., 2013). However, as shown by Schmittner et al. (2013), the effect of the calcium carbonate pump on  $\delta^{13}\text{C}$  is small, so the choice of the value for the fractionation during calcium carbonate formation is not expected to have a big impact on the  
 290 results in the current ecosystem model with one species of calcium carbonate.

### 3.2.4 Biotic $^{14}\text{C}$

The  $^{14}\text{C}$  air sea flux is calculated in the same way as shown in Eq. (15) for  $^{13}\text{C}$ , but with the fractionation for  $^{14}\text{C}$  being twice as large as for  $^{13}\text{C}$  ( $\epsilon_{14} = 2 \cdot \epsilon_{13}$ , Zeebe and Wolf-Gladrow, 2001) and with  $R^{14}\text{C}_{\text{atm}}$  and  $R^{14}\text{C}_{\text{DIC}}$  instead of  $R^{13}\text{C}_{\text{atm}}$  and  $R^{13}\text{C}_{\text{DIC}}$ . The biological fractionation is also  
 295 the same as for  $^{13}\text{C}$ , except that  $\epsilon_{14} = 2 \cdot \epsilon_{13}$  everywhere in Sect. 3.2.3. The surface reference value for  $\text{DI}^{14}\text{C}$  for the virtual flux calculation is  $1944 \mu\text{mol m}^{-3}$ , the same as for  $\text{DI}^{13}\text{C}$  (and  $\text{DI}^{12}\text{C}$ ).

In contrast to  $^{13}\text{C}$ ,  $^{14}\text{C}$  decays in all carbon pools, following the decay equation (see Eq. (11) in Sect. 3.1.2).

To compare the model simulated  $\delta^{14}\text{C}$  values that we save as diagnostics (see Eq. 14) with published observations of  $\Delta^{14}\text{C}$ , we apply the same fractionation correction to it that is used for observations to convert  $\delta^{14}\text{C}$  to  $\Delta^{14}\text{C}$ :  
 300

$$\Delta^{14}\text{C} = \delta^{14}\text{C} - 2(\delta^{13}\text{C} + 25)(1 + \delta^{14}\text{C}/1000). \quad (27)$$

In the following we always show  $\Delta^{14}\text{C}$ .

As for the abiotic  $^{14}\text{C}$  implementation, the value of  $\Delta^{14}\text{C}_{\text{atm}}$  can be set to be a constant or it can  
305 be read in from three files (one for the Northern Hemisphere, one for the equatorial region, and one  
for the Southern Hemisphere).

### 3.3 Ecosystem driver

We added an ecosystem driver (`ecosys_driver`) to the ocean model of the CESM in order to  
make it easier to expand the model to carry additional passive tracers that require variables from  
310 the ecosystem model, without adding these additional tracers to the ecosystem model itself. The  
ecosystem driver is structured similar to the `passive_tracers` subroutine that calls all passive  
tracer modules, but it handles only the passive tracers that use the ecosystem model (see Fig. 1).  
It is called from the `passive_tracers` subroutine, and determines how many ecosystem-related  
passive tracers the model carries based on the namelist options set at buildtime. It then calls all  
315 subroutines in the ecosystem model and the related tracer modules, after being called by passive  
tracers with the corresponding tracer indices. Variables computed in the ecosystem model but used  
by other modules are shared via the new `ecosys_share` module. Only the ecosystem model  
changes the value of the variables in `ecosys_share` at this point. Other modules currently only  
read them from there, but do not modify them. With this infrastructure in place, additional tracers  
320 can be easily added without changing the ecosystem model too much. The only changes to the  
ecosystem model should be the copying of ecosystem variables to `ecosys_share` if they need to  
be shared with a new module as well as potentially the addition of new definitions and calculations  
of derived ecosystem variables that are needed but that are not currently computed in the ecosystem  
model (or not present in the required format, i.e., defined as local 2-D variables instead of a global 3-  
325 D variable). Nitrogen isotopes in the ocean model have already been added using this infrastructure  
(S. Yang, personal communication, 2014).

## 4 Results

### 4.1 Simulations and spin-up

We have performed several simulations with the new carbon-isotope enabled model. As described  
330 in Sect. 2, we used the ocean-only version of the CESM1.0.5, at a nominal  $3^\circ$  horizontal resolution,  
forced by CORE-II climatological forcing (Large and Yeager, 2009). To spin up the carbon isotopes,  
we performed spin-up simulations that lasted several thousands of years. Radiocarbon takes a long  
time (5000–15 000 years, according to Orr et al., 2000) to equilibrate, due to the long timescale of  
deep ocean ventilation.

335 The abiotic radiocarbon has been spun-up for 10 000 years using an atmospheric  $\text{CO}_2$  concentra-  
tion of 284.7 ppm and a  $\Delta^{14}\text{C}$  value of 0‰. The abiotic  $\text{DI}^{14}\text{C}$  and  $\text{DI}^{12}\text{C}$  were started from the  
standard ecosystem initial conditions, scaled to yield a global initial state of 0‰  $\Delta^{14}\text{C}$  (following

Orr et al., 2000), in order to simplify early interpretation and code verification. After 10 000 simulated years, the models satisfies the OCMIP2 surface CO<sub>2</sub> flux criteria of less than 0.01 Pg C year<sup>-1</sup>.  
340 In terms of the drift in Δ<sup>14</sup>C, 91 % of the ocean volume is spun-up to the OCMIP2 criteria of a drift of less than 0.001 ‰ year<sup>-1</sup> (compared to the required 98 % for OCMIP2). Compared to the fully-spun-up solution (obtained using a new online Newton–Krylov method, manuscript in preparation by K. Lindsay, NCAR), differences are seen in the deep ocean only.

For the biotic carbon isotopes, we spun-up the carbon isotopes for 6010 years, starting from the  
345 initial conditions of the ecosystem model, scaled to give a δ<sup>13</sup>C of 0 ‰ and a Δ<sup>14</sup>C of –100 ‰. The atmospheric CO<sub>2</sub> concentration was set to 284.7 ppm, the atmospheric Δ<sup>14</sup>C was set to 0 ‰, and the atmospheric δ<sup>13</sup>C was set to –6.379 ‰. In order to study the different biological fractionation parameterizations, two additional spin-up simulations were branched from the first spin-up simulation at year 2560 and run to year 6010. After 6010 years, the surface CO<sub>2</sub> flux is well below the  
350 OCMIP2 criteria of less than 0.01 Pg C year<sup>-1</sup>, and over 99.99 % of the ocean volume show a drift of less than 0.001 ‰ year<sup>-1</sup> in δ<sup>13</sup>C. However, only 26 % of the ocean satisfies the OCMIP2 criteria of a drift of less than 0.001 ‰ year<sup>-1</sup> for Δ<sup>14</sup>C. Another 4000 years or more are likely required to get the biotic Δ<sup>14</sup>C fully spun-up according to the OCMIP2 criteria. However, if we weaken the OCMIP2 criteria by an order of magnitude to less than 0.01 ‰ year<sup>-1</sup>, 99.98 % of the ocean  
355 satisfy this new criteria for Δ<sup>14</sup>C. Due to the long time required to run the ocean model with the ecosystem and the biotic carbon isotopes (the 6010 years took over 7 months of constant running on a supercomputer), we are currently not able to run the biotic radiocarbon to full equilibrium. In order to reach equilibrium in the future, a fast spin-up technique for the ecosystem model is currently in development by Keith Lindsay and will be applied to the biotic carbon isotopes when it is ready. We  
360 believe that for the purpose of this paper, which documents the implementation of the carbon isotopes in the model, the current spin-up is sufficient, in particular because future science applications will use the fully-coupled 1°CESM, rather than the 3° ocean-only model version used here for model development. For these future science applications, the biotic radiocarbon should be spun up further in order to be fully trustworthy, and the carbon isotope simulation should be carefully validated in  
365 this model configuration.

After the long spin-up, we then performed experiments from 1765 to 2008, with the initial conditions from the end of the spin-up simulations in year 6010 for the biotic carbon isotopes and in year 10 000 for the abiotic radiocarbon. The atmospheric CO<sub>2</sub>, Δ<sup>14</sup>C, and δ<sup>13</sup>C was prescribed based on the OCMIP-2 files (Orr et al., 2000) up to 1989, and H. Graven’s formulation of the global average for 1990–2008 (personal communication, 2012). The atmospheric state was the same repeating  
370 climatological CORE-II forcing as used for the spin-up, so changes related to warming or changes in the wind forcing over the 20th century are not included. We continued with the climatological CORE-II forcing rather than use the interannually varying CORE-II forcing for 1948–2007 in order to avoid shocks to the ocean when switching the forcing and when the forcing jumps from 2007

375 back to 1948 every 60 years. This jump in the forcing impacts the simulation for 10 years or more  
(as described in Danabasoglu et. al., 2014), and would overlap with the start of the introduction of  
bomb radiocarbon into the atmosphere.

We also continued the spin-up simulations for 243 years, so that we could remove the influence  
of any continuing drift on the radiocarbon results shown in Sect. 4.2.2. To investigate the influence  
380 of the net CO<sub>2</sub> uptake on the simulation results in the second part of the 20th century, we also  
performed sensitivity experiments where the atmospheric CO<sub>2</sub> was fixed at 1949 conditions, while  
 $\Delta^{14}\text{C}_{\text{atm}}$  and  $\delta^{13}\text{C}_{\text{atm}}$  changed as usual.

## 4.2 <sup>14</sup>C results

### 4.2.1 Simulated distributions of $\Delta^{14}\text{C}$

385 The radiocarbon simulation shows good agreement with the gridded GLODAP data for the 1990s  
(Key et al., 2004), reflecting the main features of the  $\Delta^{14}\text{C}$  distribution: (i) at the surface (see Fig. 2)  
the model shows the observed M-shape of  $\Delta^{14}\text{C}$  distribution, with the highest values in the relatively  
stable subtropical waters, intermediate values in the equatorial upwelling zone, and low values in the  
polar regions, where the residence time is short and sea ice limits the uptake of atmospheric  $\Delta^{14}\text{C}$ ,  
390 with the overall lowest values in the Southern Ocean, where the upwelling of old, low  $\Delta^{14}\text{C}$  waters  
further dilutes the surface waters. (ii) In the zonal mean (see Fig. 3), newly formed deepwater with  
high  $\Delta^{14}\text{C}$  values can clearly be separated from old water masses with low  $\Delta^{14}\text{C}$  values. (iii) In the  
depth profiles (see Fig. 4), it is obvious that the  $\Delta^{14}\text{C}$  in the deep water decreases from the Atlantic  
Ocean over the Indian Ocean to the Pacific Ocean, which has the lowest  $\Delta^{14}\text{C}$  values (i.e., oldest  
395 water). Consistently, the abiotic  $\Delta^{14}\text{C}$  values are higher than the biotic  $\Delta^{14}\text{C}$  values, but both show  
the same general features also shown in GLODAP (Key et al., 2004) and in the cruise data compiled  
by Schmittner et al. (2013) because their distribution is set mainly by the physical ocean simulation.  
The difference between the abiotic and biotic simulation due to biological effects has been estimated  
to be on the order of 10% (Fiadiero, 1982), but since the biotic radiocarbon simulation is less spun-  
400 up than the abiotic simulation at this point, a detailed investigating of the impact of the biological  
effects is premature and will be the topic of a future study when we can spin-up both radiocarbon  
implementations using a fast-spin up technique.

Above 1000 m, the depth structure of the simulated  $\Delta^{14}\text{C}$  agrees reasonably well with observa-  
tions, with the best agreement with the GLODAP  $\Delta^{14}\text{C}$  in the upper 250 m of the Indian Ocean (see  
405 Fig. 4). The largest biases are found at depth below 1000 m (see Fig. 4), with the model showing  
 $\Delta^{14}\text{C}$  values that are too negative (i.e., water that is too old). The largest bias is located in the deep  
Pacific, where the  $\Delta^{14}\text{C}$  is up to 100‰ too negative (see Figs. 3 and 4). In terms of radiocarbon  
age, the maximum bias in the deep Pacific is 1000 years compared to GLODAP, revealing that the  
deep Pacific Ocean in the model is not ventilated as much as it should be. This is a well known bias

410 in the CESM, which was also present in the ocean model of a previous version of the CESM, the  
CCSM3 (Graven et al., 2012), as well as in the nominal 1° resolution version of the current CESM1  
ocean model (Bardin et al., 2014), and is related to too weak Antarctic Bottom Water formation in  
the CESM (Danabasoglu et al., 2011) and too shallow mixed layers in the Southern Ocean (Moore  
et al., 2013). Currently radiocarbon is being used to test improvements to the ventilation in the  
415 Southern Ocean in the ocean model in the CESM, in order to improve this bias in future versions of  
the CESM (K. Lindsay, personal communication, 2014).

#### 4.2.2 <sup>14</sup>C bomb inventory

The excess oceanic radiocarbon inventory is frequently used to investigate the ocean uptake of an-  
thropogenic carbon (e.g. Key et al., 2004; Graven et al., 2012) and to determine the mean gas ex-  
420 change velocity used in ocean models (e.g. Wanninkhof, 1992; Sweeney et al., 2007; Naegler et al.,  
2006; Naegler, 2009). To establish how well the newly developed radiocarbon tracer compares to  
observations, we here compare the simulated excess radiocarbon inventory with observational es-  
timates. The excess radiocarbon in the ocean includes change in the oceanic radiocarbon from the  
atmospheric nuclear bomb tests of the 1950s and 1960s, as well as from the Suess effect and changes  
425 in net CO<sub>2</sub> uptake, compared to the reference period of the 1940s, following Naegler (2009). In  
1975, the excess radiocarbon inventory in the abiotic and biotic simulation is  $297 \times 10^{26}$  atoms <sup>14</sup>C  
and  $295 \times 10^{26}$  atoms <sup>14</sup>C, respectively. This lies within the range of observational estimates of the  
excess radiocarbon in 1975, which range from  $225 \times 10^{26}$  atoms <sup>14</sup>C to  $314 \pm 35 \times 10^{26}$  atoms <sup>14</sup>C  
(see Table 2). It has been shown that the earlier estimates from Broecker et al. (1985, 1995) were  
430 high by about 25 % (e.g. Hesshaimer et al., 1994; Peacock, 2004; Sweeney et al., 2007), which sug-  
gests that the simulated values are probably on the high end of the observational range. One reason  
for this could be the choice of the coefficient  $a = 0.31 \text{ cm h}^{-1}$  in Eq. (3), which has been shown to  
be high (e.g. Sweeney et al., 2007; Naegler, 2009). Graven et al. (2012) showed that in the ocean  
model of the CCSM3, the simulated excess radiocarbon inventory was lower when a coefficient  
435  $a = 0.23 \text{ cm h}^{-1}$  rather than  $a = 0.31 \text{ cm h}^{-1}$  was used in Eq. (3). However, since  $a = 0.31 \text{ cm h}^{-1}$   
is the parameter used in the CESM in general to compute air–sea gas fluxes, we did not change it  
here. For 1995, the excess radiocarbon inventories in the abiotic and biotic simulation are  $389 \times 10^{26}$   
atoms <sup>14</sup>C and  $390 \times 10^{26}$  atoms <sup>14</sup>C, respectively, which is close to but slightly higher than the ob-  
servational estimates of  $313\text{--}383 \times 10^{26}$  atoms <sup>14</sup>C (see Table 2).

440 The natural radiocarbon inventory, before anthropogenic disturbances from the Suess effect and  
from increased oceanic net CO<sub>2</sub> uptake, has been estimated to be  $19000 \pm 1200 \times 10^{26}$  atoms of  
<sup>14</sup>C (Naegler, 2009). In the simulation the inventory is just outside the error bar for the biotic model  
( $17763\text{--}17770 \times 10^{26}$  atoms of <sup>14</sup>C, depending on the biological fractionation used), and slightly  
lower for the abiotic model ( $16190 \times 10^{26}$  atoms of <sup>14</sup>C). The natural radiocarbon inventories are  
445 calculated for years 6185–6194 of the control simulations, which corresponds to the same total

runtime as years 1940–1949 in the 1765–2008 experiments, which were started from the control in year 6010. However, the biotic model estimate of the natural radiocarbon inventory might still not be the final value, as the biotic radiocarbon is still spinning-up. In terms of the anthropogenic radiocarbon inventories presented next, this biases should not play any large role, however, as we  
450 remove any remaining drift. Specifically, to calculate the early anthropogenic radiocarbon inventory present in the 1940s, we take the difference between the natural radiocarbon inventory in simulation years 6185–6194 (with constant atmospheric  $\text{CO}_2$ ,  $\Delta^{14}\text{C}$ , and  $\delta^{14}\text{C}$ ) and the inventory in the 1940s (with changing atmospheric  $\text{CO}_2$ ,  $\Delta^{14}\text{C}$ , and  $\delta^{14}\text{C}$  since 1765). By taking this difference between years of equal total runtime, we remove the impact of any remaining drift in  $\Delta^{14}\text{C}$ . We find an  
455 anthropogenic radiocarbon inventory of  $20 \times 10^{26}$  atoms of  $^{14}\text{C}$  for the abiotic model and  $5 \times 10^{26}$  atoms of  $^{14}\text{C}$  for the biotic model (independent of the biological fractionation used). Both of these anthropogenic radiocarbon inventories for the 1940s are within the error bar of the estimate of  $4 \pm 20 \times 10^{26}$  of  $^{14}\text{C}$  from Naegler (2009), with the biotic model giving a very good match.

Using sensitivity experiments from 1950–2008 with atmospheric  $\text{CO}_2$  held constant at 1949 levels  
460 but normally increasing atmospheric  $\Delta^{14}\text{C}$ , we can calculate the impact of increased ocean uptake of anthropogenic  $\text{CO}_2$  on the excess radiocarbon inventory: in 1975, the excess oceanic radiocarbon inventory relative to the 1940s due to atmospheric  $\Delta^{14}\text{C}$  changes alone (from the atmospheric bomb tests and the Suess effect) is  $282 \times 10^{26}$  atoms of  $^{14}\text{C}$  for the abiotic model and  $280 \times 10^{26}$  atoms of  
465  $^{14}\text{C}$  for the biotic model, while for 1995 the numbers are  $353 \times 10^{26}$  atoms of  $^{14}\text{C}$  and  $354 \times 10^{26}$  atoms of  $^{14}\text{C}$ , respectively. This means that the increase in net  $\text{CO}_2$  uptake contributed  $15 \times 10^{26}$  atoms of  $^{14}\text{C}$  in 1975 and  $36 \times 10^{26}$  atoms of  $^{14}\text{C}$  in 1995 compared to the 1940s (for both the abiotic and biotic models), which is 5 and 9 % of the total radiocarbon excess in these years. These changes are in excellent agreement with calculations from Naegler (2009), which showed an excess radiocarbon inventory in 1995 of  $346 \pm 98 \times 10^{26}$  atoms  $^{14}\text{C}$  due to atmospheric  $\Delta^{14}\text{C}$  changes, and  
470  $27 \pm 9 \times 10^{26}$  atoms  $^{14}\text{C}$  due to net  $\text{CO}_2$  uptake. The percentage contribution of the net  $\text{CO}_2$  uptake to the total radiocarbon excess was given as 3 % in 1975 and 8 % in 1995 in Naegler (2009), which again compares very well with our model simulation.

### 4.3 $^{13}\text{C}$ results

#### 4.3.1 Simulated $\delta^{13}\text{C}$ and the impact of different biological 475 fractionation parameterizations

In the literature, models of biological fractionation are still under debate (e.g. Keller and Morel, 1999). We therefore tested three different parameterizations of biological fractionation, to investigate the impact on the simulated  $\delta^{13}\text{C}$  (as described in Sects. 3.2.3 and 4.1). As shown in Fig. 5a, the simulated globally averaged  $\epsilon_p$  depth profiles differ when these different parameterizations are used,  
480 with  $\epsilon_p$  values ranging from 15–30. By design,  $\epsilon_p$  is the same for diatoms, diazotrophs, and small

phytoplankton when using Rau et al. (1989), while  $\epsilon_p$  shows large variations between species for the method of Keller and Morel (1999), due to the dependence on species-specific cell parameters (see Table 1). The method of Laws et al. (1995) leads to small differences between species in the surface ocean only. Below 200 m, only the  $\epsilon_p$  following Rau et al. (1989) still changes with depth (see  
485 Fig. 5a), due to the sole dependence of  $\epsilon_p$  on  $\text{CO}_2^*$  and the export of organic carbon and carbonates to depth.

The impact of the different biological fractionation choices on  $\delta^{13}\text{C}_{\text{DIC}}$  is noticeable (see Fig. 5b), with the globally-averaged  $\delta^{13}\text{C}_{\text{DIC}}$  based on  $\epsilon_p$  from Rau et al. (1989) being larger below 150 m compared to the  $\delta^{13}\text{C}_{\text{DIC}}$  from Laws et al. (1995) and Keller and Morel (1999), but slightly smaller  
490 at the surface. Despite the more complex formulation of  $\epsilon_p$  in Keller and Morel (1999) compared to Laws et al. (1995) and the significantly different  $\epsilon_p$  profiles, the resulting  $\delta^{13}\text{C}_{\text{DIC}}$  from both methods is very similar and only differs slightly at depth (most notably between 150 and 2000 m). To compare the simulated  $\delta^{13}\text{C}_{\text{DIC}}$  to the cruise data of  $\delta^{13}\text{C}_{\text{DIC}}$  compiled by Schmittner et al. (2013), we re-gridded the model output to subsample the model at the same points as covered by the cruise data.  
495 The resulting globally-averaged depth profiles are shown in Fig. 5c, and are remarkably similar to the full globally-averaged model results in Fig. 5b. Both show the expected increase in  $\delta^{13}\text{C}_{\text{DIC}}$  directly below the surface, due to the preferential uptake of the light isotope during photosynthesis, followed by the expected decrease of  $\delta^{13}\text{C}_{\text{DIC}}$  with depth due to the remineralization of the isotopically light organic material back into the water column. The model simulated global depth-profile of  $\delta^{13}\text{C}_{\text{DIC}}$   
500 lies within the error range of  $\pm 0.2\text{‰}$  around the cruise  $\delta^{13}\text{C}_{\text{DIC}}$  data between the surface and 150 m and below 1000 m, but shows smaller  $\delta^{13}\text{C}_{\text{DIC}}$  values than observed between 150 and 1000 m.

For individual basins, the model bias compared to the cruise data is smallest in the Atlantic, with the  $\delta^{13}\text{C}_{\text{DIC}}$  based on the biological fractionation from Rau et al. (1989) almost entirely within the uncertainty range of the data (see Fig. 5d). All three basins contribute to the bias seen between 150  
505 and 2000 m in the global average, with the Indian Ocean contributing the most to this bias in the upper ocean and the Pacific Ocean contributing the most at intermediate depths (see Fig. 5c–f). In general, the model simulated  $\delta^{13}\text{C}_{\text{DIC}}$  tends to be smaller than the observed  $\delta^{13}\text{C}_{\text{DIC}}$ . While the difference between the full global average in the model and the subset global average based on the cruise data locations is small, the difference between the total basin average (shown as dashed lines  
510 in Fig. 5d–f) and the subset basin averages (shown as solid lines) is larger for the individual basins.

At the surface, the simulated  $\delta^{13}\text{C}_{\text{DIC}}$  values show a systematic bias in that they are generally larger than the observational data suggests, but the same general spatial pattern is visible (see Fig. 6). While both gas-exchange and biological process are important for the surface ocean  $\delta^{13}\text{C}_{\text{DIC}}$  pattern (Schmittner et al., 2013), the details of the biological fractionation parameterizations appear to have  
515 a very small impact at the surface, as shown in the almost identical surface distributions from the model (see Fig. 6c–e). The zonal means of  $\delta^{13}\text{C}_{\text{DIC}}$  from the different biological fractionation parameterizations on the other hand do show some small differences (see Fig. 7), with the biological

fractionation from Rau et al. (1989) leading to the largest  $\delta^{13}\text{C}_{\text{DIC}}$  values in all three ocean basins, while the fractionation based on Keller and Morel (1999) shows the lowest  $\delta^{13}\text{C}_{\text{DIC}}$  values. Overall  
520 all three parameterizations lead to the expected pattern of high values of  $\delta^{13}\text{C}_{\text{DIC}}$  in water that has recently been in contact with the surface (e.g., North Atlantic Deep Water) and low  $\delta^{13}\text{C}_{\text{DIC}}$  values in water that has been out-of-contact with the atmosphere for a long period of time and has accumulated a large amount of remineralized (isotopically light) organic matter (e.g., in the deep Pacific).

We choose the biological formulation from Laws et al. (1995) as the default biological fractionation  
525 in our model, as it considers the growth rate of different species, but the differences in the simulated  $\delta^{13}\text{C}_{\text{DIC}}$  compared to the more complex formulation from Keller and Morel (1999) is small. The other parameterizations of biological fractionation remain an option in the model that can be chosen at build time.

#### 4.3.2 Oceanic surface $^{13}\text{C}$ Suess effect

530 The surface oceanic Suess effect, which is the decrease in the surface ocean  $\delta^{13}\text{C}$  due to the penetration of carbon originating from the burning of fossil fuels, has been calculated from observational data as well as from other models that include  $^{13}\text{C}$ , and it is often used to derive the oceanic anthropogenic carbon uptake (e.g. McNeil et al., 2001; Tagliabue and Bopp, 2008). In our model simulation, the surface  $\delta^{13}\text{C}$  change between 1975 and 1995 is  $-0.164$  to  $-0.167\text{‰ decade}^{-1}$   
535 (the range is for the different biological fractionations used). This compares well with other estimates of  $-0.171\text{‰ decade}^{-1}$  (Bacastow et al., 1996),  $-0.18\text{‰ decade}^{-1}$  (Gruber et al., 1999),  $-0.15\text{‰ decade}^{-1}$  (Sonnerup et al., 1999), and  $-0.174\text{‰ decade}^{-1}$  (Tagliabue and Bopp, 2008). As already shown by Quay et al. (1992) and Gruber et al. (1999), the surface ocean Suess effect is not uniform (see Fig. 8), and the model simulation of the spatial Suess effect agrees well with  
540 the model results of Tagliabue and Bopp (2008): the largest changes (i.e., most negative values in Fig. 8) occur in regions with little deep ventilation and therefore longer residence times of water at the surface (e.g., the subtropical gyres) while the smallest changes (i.e., least negative or zero in Fig. 8) occur in regions of reduced air–sea gas exchange (e.g., under sea ice), in regions with active deep convection (and therefore short residence times at the surface, e.g. around Antarctic), as well  
545 as in regions with upwelling (which dilutes the surface  $\delta^{13}\text{C}$ , for example off the west coast of South America).

Compared to the pre-industrial ocean, the total surface ocean  $^{13}\text{C}$  Suess effect is  $-0.064$  to  $-0.065\text{‰ decade}^{-1}$  for 1860–2000 (depending on the different biological fractionation used), compared to  $-0.07\text{‰ decade}^{-1}$  found by Tagliabue and Bopp (2008). The fact that the simulated  
550 oceanic  $^{13}\text{C}$  Suess effect calculated over different periods agrees reasonably well with other available estimates suggests that our model is able to simulate the change in the oceanic  $\delta^{13}\text{C}$  inventory correctly, despite some mean biases in the distribution of  $\delta^{13}\text{C}$  described and shown in Sect. 4.3.1.

## 5 Summary

We have developed carbon isotope tracers in the ocean model of the CESM, including a biotic  
555 and an abiotic radiocarbon tracer and a biotic  $^{13}\text{C}$  tracer. The details of the implementation are  
described here in order to serve as reference for future users of these new model features and/or for  
model developers planning to modify the code or add carbon isotopes to other ocean models. In  
particular, we tested three different formulations for the fractionation during phytoplankton growth  
that have been discussed in the literature, and show that the effect on the simulated  $\delta^{13}\text{C}$  in the ocean  
560 is relatively minor. A comparison of the simulation results from the coarse nominal-3° resolution  
ocean model forced with climatological CORE-II atmospheric forcing and with present-day data for  
 $\Delta^{14}\text{C}$  and  $\delta^{13}\text{C}$  shows that the simulated carbon isotopes can represent the large-scale features of  
the observed distributions as well as the anthropogenic changes due to nuclear bomb tests and the  
burning of fossil fuels. The carbon isotopes also reflect some known model biases, for example a too  
565 sluggish ventilation of the deep Pacific Ocean. Once a fast-spin up technique for the biotic carbon  
isotopes has been implemented, we are planning to further validate the carbon-isotope simulation in  
the fully-coupled CESM framework at 1° resolution. Ultimately, we plan to use the carbon isotopes  
for both present-day and paleo simulations in the fully-coupled framework of the CESM at the  
standard nominal 1° resolution in the ocean, in order to investigate details of changes in the ocean  
570 circulation over the 20th century, the last Millennium, and at the Last Glacial Maximum.

### Code availability

The newly developed carbon isotope and ecosystem driver code for the CESM1.0.5 is included as  
supplementary material here. The carbon isotope code has been updated to the CESM1.2, and has  
been added to the ocean development trunk in the CESM SVN repository (as of version cesm1-3-  
575 beta10). It continues to be updated as the CESM evolves, and is targeted for public release as part  
of the CESM2 in 2016. At that point the code will be available through the CESM release website  
at <https://www2.cesm.ucar.edu/models/current>. Prior to the release, developer access can already  
be applied for at <https://www2.cgd.ucar.edu/sections/cseg/development-code>, subject to the CESM  
development guidelines.

580 *Acknowledgements.* A. Jahn was funded under the DOE SciDAC grant “Development of an Isotope-Enabled  
CESM for Testing Abrupt Climate Changes” (DE-SC0006744). We thank Michael Levy (NCAR) and David M.  
Hall (CU Boulder) for software engineering advice, Matt Long (NCAR) for helpful discussions, and Heather  
Graven (Scripps) for sharing her extensions of the OCMIP atmospheric  $\Delta^{14}\text{C}$ ,  $\delta^{13}\text{C}$ , and  $\text{CO}_2$  data with us. We  
also thank Guy Munhoven for serving as editor and two anonymous reviewers for their constructive comments  
585 on the discussion paper. NCAR is sponsored by the National Science Foundation. N. Gruber and X. Giraud  
acknowledge funding from ETH Zürich. Computing resources (ark:/85065/d7wd3xhc) were provided by the

Climate Simulation Laboratory at NCAR's Computational and Information Systems Laboratory on Yellowstone (2012), sponsored by the National Science Foundation and other agencies. Data analysis was performed with NCL Version 6.2.0 (2014).

## 590 References

- Bacastow, R. B., Keeling, C. D., Lueker, T. J., Wahlen, M., and Mook, W. G.: The  $^{13}\text{C}$  Suess Effect in the world surface oceans and its implications for oceanic uptake of  $\text{CO}_2$ : analysis of observations at Bermuda, *Global Biogeochem. Cy.*, 10, 335–346, doi:10.1029/96GB00192, 1996.
- Bardin, A., Primeau, F., and Lindsay, K.: An offline implicit solver for simulating prebomb radiocarbon, *Ocean Modelling*, 73, 45–58, doi:10.1016/j.ocemod.2013.09.008, 2014.
- 595 Bigeleisen, J.: The effects of isotopic substitutions on the rate of chemical reactions, *J. Phys. Chem.*, 56, 823–828, 1952.
- Bohlen, L., Dale, A., and Wallmann, K.: Simple transfer functions for calculating benthic fixed nitrogen losses and C:N:P regeneration ratios in global biogeochemical models, *Global Biogeochem. Cy.*, 26, GB3029, doi:10.1029/2011GB004198, 2012.
- 600 Broecker, W. S. and Peng, T.-H.: Stratospheric contribution to the global bomb radiocarbon inventory: model versus observation, *Global Biogeochem. Cy.*, 8, 377–384, doi:10.1029/94GB00680, 1994.
- Broecker, W. S., Peng, T. H., and Engh, R.: Modelling the carbon system, *Radiocarbon*, 22, 377–384, 1980.
- Broecker, W. S., Peng, T.-H., Östlund, G., and Stuiver, M.: The distribution of bomb radiocarbon in the ocean, *J. Geophys. Res.*, 90, 6953–6970, doi:10.1029/JC090iC04p06953, 1985.
- 605 Broecker, W. S., Sutherland, S., Smethie, W., Peng, T. H., and Östlund, G.: Oceanic radiocarbon: separation of the natural and bomb components, *Global Biogeochem. Cy.*, 9, 263–288, doi:10.1029/95GB00208, 1995.
- Craig, H.: Carbon 13 in plants and the relationship between carbon 13 and carbon 14 variations in nature, *J. Geol.*, 62, 115–149, 1954.
- 610 Craig, H.: Isotopic standards for carbon and oxygen and correction factors for mass-spectrometric analysis of carbon dioxide, *Geochim. Cosmochim. Ac.*, 12, 133–149, 1957.
- Crucifix, M.: Distribution of carbon isotopes in the glacial ocean: a model study, *Paleoceanography*, 20, PA4020, doi:10.1029/2005PA001131, 2005.
- Curry, W. B. and Oppo, D. W.: Glacial water mass geometry and the distribution of  $\delta^{13}\text{C}$  of  $p\text{CO}_2$  in the Western Atlantic Ocean, *Paleoceanography*, 20, PA1017, doi:10.1029/2004PA001021, 2005.
- 615 Danabasoglu, G., S. C. Bates, B. P. Briegleb, S. R. Jayne, M. Jochum, W. G. Large, S. Peacock, and S. G. Yeager: The CCSM4 Ocean Component, *J. Climate*, 25, 1361–1389. doi:http://dx.doi.org/10.1175/JCLI-D-11-00091.1, 2012.
- Danabasoglu, G., S. G. Yeager, D. Bailey, E. Behrens, M. Bentsen, D. Bi, A. Biastoch, C. Böning, A. Bozec, V. M. Canuto, C. Cassou, E. Chassignet, A. C. Coward, S. Danilov, N. Diansky, H. Drange, R. Farneti, E. Fernandez, P. G. Fogli, G. Forget, Y. Fujii, S. M. Griffies, A. Gusev, P. Heimbach, A. Howard, T. Jung, M. Kelley, W. G. Large, A. Leboissetier, J. Lu, G. Madec, S. J. Marsland, S. Masina, A. Navarra, A. J. George Nurser, A. Pirani, D. Salas y Melia, B. L. Samuels, M. Scheinert, D. Sidorenko, A.-M. Treguier, H. Tsujino, P. Uotila, S. Valcke, A. Voldoire, Q. Wang: North Atlantic simulations in Coordinated Ocean-ice Reference Experiments phase {II} (CORE-II). Part I: Mean states, *Ocean Modelling*, 73, 76–107, doi:http://dx.doi.org/10.1016/j.ocemod.2013.10.005, 2014.
- 625 Doney, S. C., Lindsay, K., Caldeira, K., Campin, J., Drange, H., Dutay, J., Follows, M., Gao, Y., Gnanadesikan, A., Gruber, N., Ishida, A., Joos, F., Madec, G., Maier-Reimer, E., Marshall, J., Matear, R., Monfray, P., Mouchet, A., Najjar, R., Orr, J., Plattner, G., Sarmiento, J., Schlitzer, R., Slater, R., Totterdell, I., Weirig, M.,

- 630 Yamanaka, Y., and Yool, A.: Evaluating global ocean carbon models: the importance of realistic physics, *Global Biogeochem. Cy.*, 18, GB3017, doi:10.1029/2003GB002150, 2004.
- Dunne, J. P., Sarmiento, J. L., and Gnanadesikan, A.: A synthesis of global particle export from the surface ocean and cycling through the ocean interior and on the seafloor, *Global Biogeochem. Cy.*, 21, GB4006, doi:10.1029/2006GB002907, 2007.
- 635 Fiadiero, M. E.: Three-dimensional modeling of tracers in the deep Pacific Ocean: radiocarbon and the circulation, *J. Mar. Res.*, 40, 537–550, 1982.
- Galbraith, E. D., Kwon, E. Y., Gnanadesikan, A., Rodgers, K. B., Griffies, S. M., Bianchi, D., Sarmiento, J. L., Dunne, J. P., Simeon, J., Slater, R. D., Wittenberg, A. T., and Held, I. M.: Climate variability and radiocarbon in the CM2Mc Earth System Model, *J. Climate*, 24, 4230–4254, doi:10.1175/2011JCLI3919.1, 2011.
- 640 Godwin, H.: Half life of radiocarbon, *Nature*, 195, 984, doi:10.1038/195984a0, 1962.
- Goericke, R., Montoya, J. P., and Fry, B.: Physiology of isotopic fractionation in algae and cyanobacteria, in: *Stable Isotopes in Ecology and Environmental Science*, edited by: Lajtha, K. and Michener, R. H., Blackwell Scientific Publications, Oxford, 187–221, 1994.
- Graven, H. D., Gruber, N., Key, R., Khatiwala, S., and Giraud, X.: Changing controls on oceanic radiocarbon: new insights on shallow-to-deep ocean exchange and anthropogenic CO<sub>2</sub> uptake, *J. Geophys. Res.*, 117, C10005, doi:10.1029/2012JC008074, 2012.
- 645 Gruber, N. and Keeling, C. D.: The isotopic air–sea disequilibrium and the oceanic uptake of CO<sub>2</sub>, in: *Proceedings of the 2nd International Symposium CO<sub>2</sub> in the oceans*, NIS, Tsukuba, Japan, edited by: Nojiri, Y., CGER-I037, Center for Global Environmental Research, National Institute for Environmental Studies, 245–
- 650 250, 1999.
- Gruber, N. and Keeling, C.: An improved estimate of the isotopic air–sea disequilibrium of CO<sub>2</sub>: implications for the oceanic uptake of anthropogenic CO<sub>2</sub>, *Geophys. Res. Lett.*, 28, 555–558, 2001.
- Gruber, N., Keeling, C. D., Bacastow, R. B., Guenther, P. R., Leucker, T. J., Wahlen, M., Meijer, H. A. J., Mook, W. G., and Stocker, T. F.: Spatiotemporal patterns of carbon-13 in the global surface oceans and the
- 655 oceanic Suess effect, *Global Biogeochem. Cy.*, 13, 307–335, 1999.
- Hesse, T., Butzin, M., Bickert, T., and Lohmann, G.: A model-data comparison of  $\delta^{13}\text{C}$  in the glacial Atlantic Ocean, *Paleoceanography*, 26, PA3220, doi:10.1029/2010PA002085, 2011.
- Hesshaimer, V., Heimann, M., and Levin, I.: Radiocarbon evidence for a smaller oceanic carbon dioxide sink than previously believed, *Nature*, 370, 201–203, doi:10.1038/370201a0, 1994.
- 660 Hurrell, J., Holland, M. M., Ghan, P. R. G. S., Kushner, J. K. P., Lamarque, J.-F., Large, W. G., D. Lawrence, D., Lindsay, K., Lipscomb, W. H., Long, M., Mahowald, N., Marsh, D., Neale, R., Rasch, P., Vavrus, S., Vertenstein, M., Bader, D., Collins, W. D., Hack, J. J., Kiehl, J., and Marshall, S.: The Community Earth System Model: a framework for collaborative research, *B. Am. Meteorol. Soc.*, 94, 1339–1360, doi:10.1175/BAMS-D-12-00121.1, 2013.
- 665 Karlen, I., Olsson, I. U., Kallburg, P., and Kilici, S.: Absolute determination of the activity of two <sup>14</sup>C dating standards, *Ark. Geofys.*, 4, 465–471, 1968.
- Keeling, C. D., Bacastow, R. B., and Tans, P. P.: Predicted shift in the <sup>13</sup>C/<sup>12</sup>C ratio of atmospheric carbon dioxide, *Geophys. Res. Lett.*, 7, 505–508, doi:10.1029/GL007i007p00505, 1980.
- Keller, K. and Morel, F. M. M.: A model of carbon isotopic fractionation and active carbon uptake in phyto-

- 670 plankton, *Mar. Ecol.-Prog. Ser.*, 182, 295–298, 1999.
- Key, R. M., Kozyr, A., Sabine, C. L., Lee, K., Wanninkhof, R., Bullister, J. L., Feely, R. A., Millero, F. J., Mordy, C., and Peng, T.-H.: A global ocean carbon climatology: results from Global Data Analysis Project (GLODAP), *Global Biogeochem. Cy.*, 18, GB4031, doi:10.1029/2004GB002247, 2004.
- Large, W. G. and Yeager, S. G.: The global climatology of an interannually varying air–sea flux data set, *Clim. Dynam.*, 33, 341–364, doi:10.1007/s00382-008-0441-3, 2009.
- 675 Lassey, K. R., Manning, M. R., and O’Brien, B. J.: An overview of oceanic radiocarbon: its inventory and dynamics, *CRC Rev. Aquatic Sci.*, 3, 117–146, 1990.
- Laws, E. A., Bidigare, R. R., and Popp, B. N.: Effect of growth rate and CO<sub>2</sub> concentration on carbon isotopic fractionation by the marine diatom *Phaeodactylum tricornutum*, *Limnol. Oceanogr.*, 42, 1552–1560, 1997.
- 680 Laws, E. A., Popp, B. N., Bidigare, R. R., Kennicutt, M. C., and Macko, S. A.: Dependence of phytoplankton carbon isotopic composition on growth rate and [CO<sub>2</sub>]<sub>aq</sub>: theoretical considerations and experimental results, *Geochim. Cosmochim. Ac.*, 59, 1131–1138, doi:10.1016/0016-7037(95)00030-4, 1995.
- Libby, W. F.: *Radiocarbon Dating*, 2nd edn., Univ. Chicago Press, 1955.
- Marchal, O., Stocker, T. F., and Joos, F.: A latitude-depth, circulation-biogeochemical ocean model for paleo-  
685 climate studies. Development and sensitivities, *Tellus B*, 50, 290–316, doi:10.1034/j.1600-0889.1998.t01-2-00006.x, 1998.
- Matsumoto, K., Sarmiento, J. L., Key, R. M., Aumont, O., Bullister, J. L., Caldeira, K., Campin, J., Doney, S. C., Drange, H., Dutay, J.-C., Follows, M., Gao, Y., Gnanadesikan, A., Gruber, N., Ishida, A., Joos, F., Lindsay, K., Maier-Reimer, E., Marshall, J., Matear, R., Monfray, P., Mouchet, A., Najjar, R.,  
690 Plattner, G., Schlitzer, R., Slater, R., Swathi, P., Totterdell, I., Weirig, M., Yamanaka, Y., Yool, A., and Orr, J.: Evaluation of ocean carbon cycle models with data-based metrics, *Geophys. Res. Lett.*, 31, L07303, doi:10.1029/2003GL018970, 2004.
- McDermott, F.: Palaeo-climate reconstruction from stable isotope variations in speleothems: a review, *Quaternary Sci. Rev.*, 23, 901–918, doi:10.1016/j.quascirev.2003.06.021, 2004.
- 695 McNeil, B. I., Matear, R. J., and Tilbrock, B.: Does carbon 13 track anthropogenic CO<sub>2</sub> in the Southern Ocean?, *Global Biogeochem. Cy.*, 15, 597–613, 2001.
- Meissner, K. J.: Younger Dryas: a data to model comparison to constrain the strength of the overturning circulation, *Geophys. Res. Lett.*, 34, L21705, doi:10.1029/2007GL031304, 2007.
- Meissner, K. J., Schmittner, A., Weaver, A. J., and Adkins, J. F.: Ventilation of the North Atlantic Ocean during  
700 the Last Glacial Maximum: a comparison between simulated and observed radiocarbon ages, *Paleoceanography*, 18, 1023, doi:10.1029/2002PA000762, 2003.
- Mook, W. G.: <sup>13</sup>C in atmospheric CO<sub>2</sub>, *Neth. J. Sea Res.*, 20, 211–223, 1986.
- Moore, J. K., Lindsay, K., Doney, S. C., Long, M. C., and Misumi, K.: Marine ecosystem dynamics and biogeochemical cycling in the Community Earth System Model [CESM1(BGC)]: comparison of the 1990s  
705 with the 2090s under the RCP4.5 and RCP8.5 scenarios, *J. Climate*, 26, 9291–9312, doi:10.1175/JCLI-D-12-00566.1, 2013.
- Naegler, T.: Reconciliation of excess <sup>14</sup>C-constrained global CO<sub>2</sub> piston velocity estimates, *Tellus B*, 61, 372–384, 2009.
- Naegler, T. and Levin, I.: Closing the global radiocarbon budget 1945–2005, *J. Geophys. Res.*, 111, D12311,

- 710 doi:10.1029/2005JD006758, 2006.
- Naegler, T., Ciais, P., Rodgers, K., and Levin, I.: Excess radiocarbon constraints on air–sea gas exchange and the uptake of CO<sub>2</sub> by the oceans, *Geophys. Res. Lett.*, 33, L11802, doi:10.1029/2005GL025408, 2006.
- NCL Version 6.2.0, Boulder, C. U.: The NCAR Command Language, doi:10.5065/D6WD3XH5, 2014.
- O’Leary, M. H.: Measurement of the isotope fractionation associated with diffusion of carbon dioxide in aqueous solution, *J. Phys. Chem.*, 88, 823–825, 1984.
- 715 Orr, J. C.: Global Ocean Storage of Anthropogenic Carbon (GOSAC), Tech. rep., EC Environment and Climate Program, Final Report, 2002.
- Orr, J., Najjar, R., Sabine, C., and Joos, F.: Abiotic-HOWTO, Technical report, revision: 1.16, available at: <http://ocmip5.ipsl.jussieu.fr/OCMIP/phase2/simulations/Abiotic/HOWTO-Abiotic.html> (last access: 15
- 720 May 2012), 2000.
- Peacock, S.: Debate over the ocean bomb radiocarbon sink: closing the gap, *Global Biogeochem. Cy.*, 18, GB2022, doi:10.1029/2003GB002211, 2004.
- Petit, J. R., Jouzel, J., Raynaud, D., Barkov, N. I., Barnola, J.-M., Basile, I., Bender, M., Chappellaz, J., Davis, M., G. D., Delmotte, M., Kotlyakov, V. M., Legrand, M., Lipenkov, V. Y., Lorius, C., Pepin, L.,
- 725 Ritz, C., Saltzman, E., and Stievenard, M.: Climate and atmospheric history of the past 420,000 years from the Vostok ice core, Antarctica, *Nature*, 399, 429–436, 1999.
- Polka, J. S., van Beynenb, P., Asmeromc, Y., and Polyakc, V. J.: Reconstructing past climates using carbon isotopes from fulvic acids in cave sediments, *Chem. Geol.*, 360–361, 1–9, doi:10.1016/j.chemgeo.2013.09.022, 2013.
- 730 Popp, B. N., Laws, E. A., Ridigare, R. R., Dore, J. E., Hanson, K. L., and Wakeham, S. G.: Effect of phytoplankton cell geometry on carbon isotope fractionation, *Geochim. Cosmochim. Ac.*, 62, 69–77, 1998.
- Quay, P. D., Tilbrook, B., and Wong, C. S.: Oceanic uptake of fossil fuel CO<sub>2</sub>: carbon-13 evidence, *Science*, 256, 74–79, 1992.
- Rau, G. H., Takahashi, T., and Marais, D. J. D.: Latitudinal variations in plankton  $\delta^{13}\text{C}$ : implications for CO<sub>2</sub>
- 735 and productivity in past oceans, *Nature*, 341, 516–518, 1989.
- Raymond, P. A., Bauerb, J. E., Caracoc, N. F., Colec, J. J., Longworthd, B., and Petschd, S. T.: Controls on the variability of organic matter and dissolved inorganic carbon ages in northeast US rivers, *Mar. Chem.*, 92, 353–366, 2004.
- Schmittner, A., Gruber, N., Mix, A. C., Key, R. M., Tagliabue, A., and Westberry, T. K.: Biology and air–sea
- 740 gas exchange controls on the distribution of carbon isotope ratios ( $\delta^{13}\text{C}$ ) in the ocean, *Biogeosciences*, 10, 5793–5816, doi:10.5194/bg-10-5793-2013, 2013.
- Shields, C. A., Bailey, D. A., Danabasoglu, G., Jochum, M., Kiehl, J. T., Levis, S., and Park, S.: The low-resolution CCSM4, *J. Climate*, 25, 3993–4014, doi:10.1175/JCLI-D-11-00260.1, 2012.
- Sikes, C. S., Roer, R. D., and Wilbur, K. M.: Photosynthesis and coccolith formation: inorganic carbon sources
- 745 and net inorganic reaction of deposition, *Limnol. Oceanogr.*, 25, 248–261, 1980.
- Soetaert, K., Herman, P. M. J., and Middelburg, J. J.: A model of early diagenetic processes from the shelf to abyssal depths, *Geochim. Cosmochim. Ac.*, 60, 1019–1040, doi:10.1016/0016-7037(96)00013-0, 1996.
- Sonnerup, R. E., Quay, P. D., McNichol, A. P., Bullister, J. L., Westby, T. A., and Anderson, H. L.: Reconstructing the ocean <sup>13</sup>C Suess effect, *Global Biogeochem. Cy.*, 13, 857–872, doi:10.1029/1999GB900027,

**Table 1.** Parameters used in the parameterization of  $\epsilon_p$  for the implementation following Keller and Morel (1999). The values for small phytoplankton are based on *E. huxleyi*, the value for diatoms are based on *P. tricornutum*, and the values for diatoms are based on *Synechococcus* sp. (Keller and Morel, 1999; Popp et al., 1998).

	Small phytoplankton	Diatom	Diazotroph
Qc [mol C cell <sup>-1</sup> ]	$69.2 \times 10^{-14}$	$63.3 \times 10^{-14}$	$3 \times 10^{-14}$
cell <sub>permea</sub> [m s <sup>-1</sup> ]	$1.8 \times 10^{-5}$	$3.3 \times 10^{-5}$	$3.0 \times 10^{-8}$
cell <sub>surf</sub> [m <sup>2</sup> ]	$87.6 \times 10^{-12}$	$100.6 \times 10^{-12}$	$5.8 \times 10^{-12}$
C <sub>up</sub>	2.2	2.3	7.5
$\epsilon_{\text{fix}}$	25.3	26.6	30

- 750 1999.
- Stuiver, M. and Polach, H. A.: Discussion: reporting of <sup>14</sup>C Data, Radiocarbon, 19, 355–363, 1977.
- Sweeney, C., Gloor, E., Jacobson, A. R., Key, R. M., McKinley, G., Sarmiento, J. L., and Wanninkhof, R.: Constraining global air–sea gas exchange for CO<sub>2</sub> with recent bomb <sup>14</sup>C measurements, Global Biogeochem. Cy., 21, GB2015, doi:10.1029/2006GB002784, 2007.
- 755 Tagliabue, A. and Bopp, L.: Towards understanding global variability in ocean carbon-13, Global Biogeochem. Cy., 22, GB1025, doi:10.1029/2007GB003037, 2008.
- Toggweiler, J. R., Dixon, K., and Bryan, K.: Simulations of radiocarbon in a coarse-resolution world ocean model 1. Steady state prebomb distributions, J. Geophys. Res., 94, 8217–8242 doi:10.1029/JC094iC06p08217, 1989.
- 760 Tortell, P. D., Reinfelder, J. R., and More, F. M. M.: Active uptake of bicarbonate by diatoms, Nature, 390, 243–244, 1997.
- Turner, J. V.: Kinetic fractionation of <sup>13</sup>C during calcium carbonate precipitation, Geochim. Cosmochim. Ac., 46, 1183–1191, doi:10.1016/0016-7037(82)90004-7, 1982.
- Wanninkhof, R.: Relationship between wind speed and gas exchange over the ocean, J. Geophys. Res., 97, 7373–7382, 1992.
- 765 Waugh, D. W., Hall, T. M., and Haine, T. W. N.: Relationships among tracer ages, J. Geophys. Res., 108, 3138, doi:10.1029/2002JC001325, 2003.
- Yellowstone: Computational and Information Systems Laboratory, National Center for Atmospheric Research, Boulder, CO, Yellowstone: IBM iDataPlex System (Climate Simulation Laboratory), available at: <http://n2t.net/ark:/85065/d7wd3xhc> (last access: 15 September 2014), 2012.
- 770 Zeebe, R. E. and Wolf-Gladrow, D.: CO<sub>2</sub> in Seawater: Equilibrium, Kinetic, Isotopes, 3rd Edn., Elsevier Oceanography Series 65, Elsevier Ltd, 2001.
- Zhang, J., Quay, P. D., and Wilbur, D. O.: Carbon isotope fractionation during gas-water exchange and dissolution of CO<sub>2</sub>, Geochim. Cosmochim. Ac., 59, 107–114, 1995.
- 775 Ziveri, P., Stoll, H. M., Probert, I., Klaas, C., Geisen, M., J., J. Y., and Ganssen, G.: Stable isotope vital effects in coccolith calcite, Earth Planet. Sc. Lett., 210, 137–149, 2003.

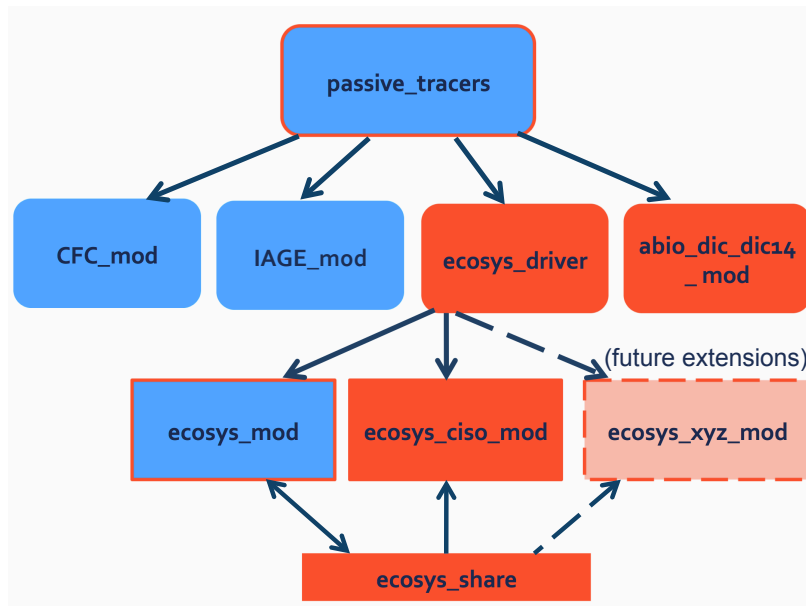


**Fig. 1.** Schematic of the passive tracer modules with the new ecosystem driver and carbon isotope modules. Existing modules are shown in blue, new modules are shown in red, and edited modules are shown in blue with a red box. Dashed lines indicate future developments. This schematic shows how the ecosystem driver acts as an interface between the ecosystem-related modules and the passive tracers module that drives all tracer modules as well as how *ecosys\_share* is used to share variables computed by the ecosystem model and used by other modules beside the ecosystem model.

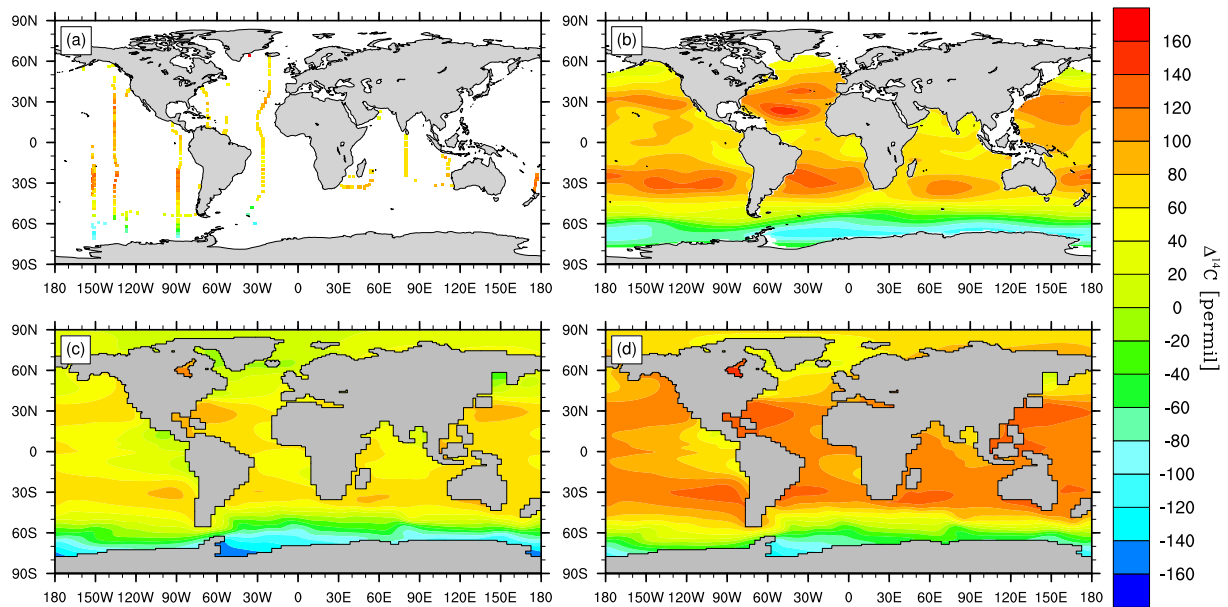


**Fig. 2.** Surface values of total  $\Delta^{14}\text{C}$  from the 1990s (including bomb  $^{14}\text{C}$ ) from (a) cruise data compiled by Schmittner et al. (2013), (b) the gridded GLODAP data (Key et al., 2004), (c) simulated biotic  $\Delta^{14}\text{C}$ , and (d) simulated abiotic  $\Delta^{14}\text{C}$ .

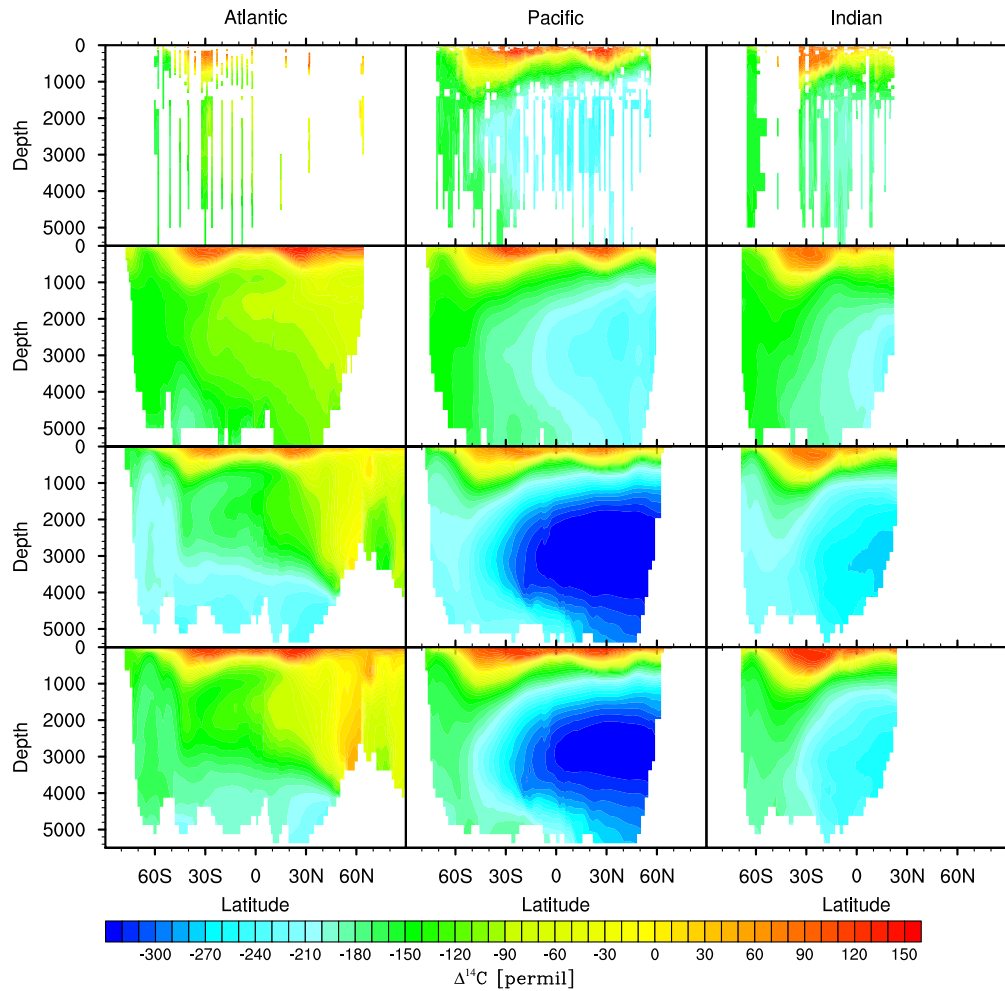


**Fig. 3.** Zonal averages of total  $\Delta^{14}\text{C}$  for the Atlantic, Pacific, and Indian Ocean for the 1990s, from cruise data compiled by Schmittner et al. (2013) (top row), the gridded GLODAP data (Key et al., 2004) (second row), the  $\Delta^{14}\text{C}$  from the biotic model (third row), and the abiotic model (bottom row). Note that due to the sparse observational data (see Fig. 2a for the coverage at the surface), the zonal average from the cruise data in the top row is more of a zonal composite than a zonal average.

**Table 2.** Excess oceanic radiocarbon inventory, measured in  $10^{26}$  atoms of  $^{14}\text{C}$ , from various sources for 1975 (GEOSECS) and 1995 (WOCE). Corrections by Naegler et al. (2006) are for neglected ocean regions, corrections by Naegler (2009) are for neglected contributions from increasing DIC. The values from this study are listed at the bottom, for the abiotic and biotic implementation. The biotic excess radiocarbon inventories are the same for all biological fractionation choices tested.

Publication	1975 (GEOSECS)	1995 (WOCE)
Broecker et al. (1980)	$314 \pm 35$	
Broecker et al. (1985)	289	
Lasley et al. (1990)	303	
Hesshaimer et al. (1994)	225	
Broecker and Peng (1994)	300	
Broecker et al. (1995)	$305 \pm 30$	
Peacock (2004) multitracer correlation	$241 \pm 60$	$335 \pm 15$
corrected by Naegler et al. (2006)	$245 \pm 60$	$340 \pm 15$
corrected by Naegler (2009)	$252 \pm 60$	$367 \pm 15$
Peacock (2004) silicate approach	$262 \pm 26$	
corrected by Naegler et al. (2006)	$264 \pm 26$	
Key et al. (2004)		$313 \pm 47$
corrected by Naegler et al. (2006)		$355 \pm 50$
corrected by Naegler (2009)		$383 \pm 50$
Naegler and Levin (2006)	$258 \pm 13$	$367 \pm 17$
Sweeney et al. (2007)	225	$343 \pm 40$
corrected by Naegler (2009)	232	$370 \pm 40$
Naegler (2009)		$373 \pm 98$
This study, abiotic $^{14}\text{C}$	297	389
This study, biotic $^{14}\text{C}$	295	390

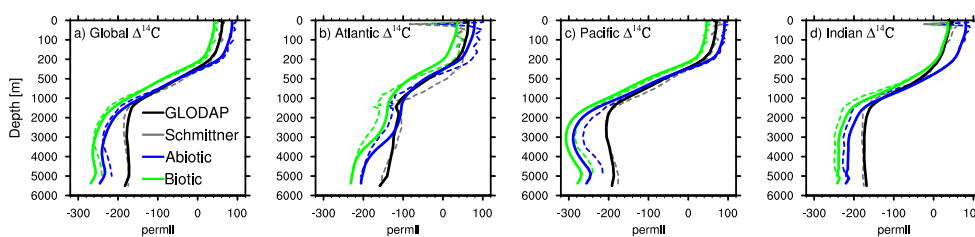


**Fig. 4.** Depth profiles of  $\Delta^{14}\text{C}$  for (a) the global ocean, (b) the Atlantic Ocean, (c) the Pacific Ocean, and (d) the Indian Ocean. The simulated biotic (green) and abiotic (blue)  $\Delta^{14}\text{C}$  is compared to the global gridded GLODAP  $\Delta^{14}\text{C}$  (black) dataset (Key et al., 2004). In addition dashed lines show the cruise data compiled by Schmittner et al. (2013) (gray) and the model simulated data subsampled at the same locations as this data (green and blue dashed lines).

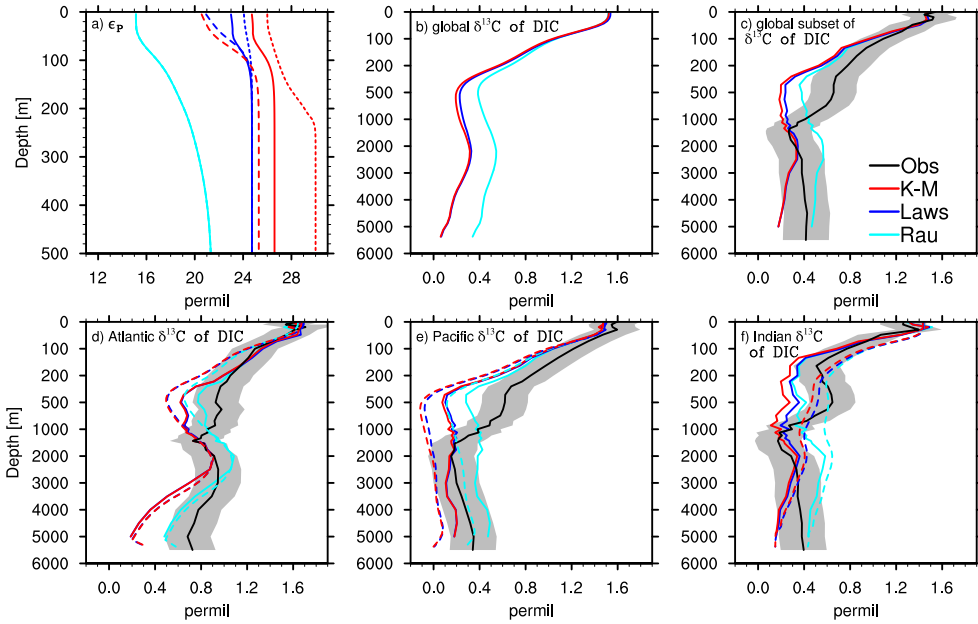


**Fig. 5.** (a) Depth profiles over the top 500 m (where  $\epsilon_p$  is important because of primary production) of the globally-averaged values of  $\epsilon_p$  produced by the three tested parameterizations for biological fractionation for diatoms (solid line), diazotrophs (short dashes), and small phytoplankton (large dashes). The simulated globally-averaged depth profile (0–6000 m) of  $\delta^{13}\text{C}_{\text{DIC}}$  in the 1990s is shown in (b), and the global average depth profile of the subset model  $\delta^{13}\text{C}_{\text{DIC}}$  for the same grid points as in the cruise data compiled by Schmittner et al. (2013) is shown in (c). Basin average depth-profiles are shown in (d–f), with dashed lines showing the full basin average from the model and solid lines showing the subset averages for the same points as the cruise data compiled by Schmittner et al. (2013). The uncertainty for the cruise data is shown as grey shading in (c), and is  $\pm 0.2\%$  (Schmittner et al., 2013). Note that the irregular  $y$  axis in (b–f) emphasizes the upper ocean.

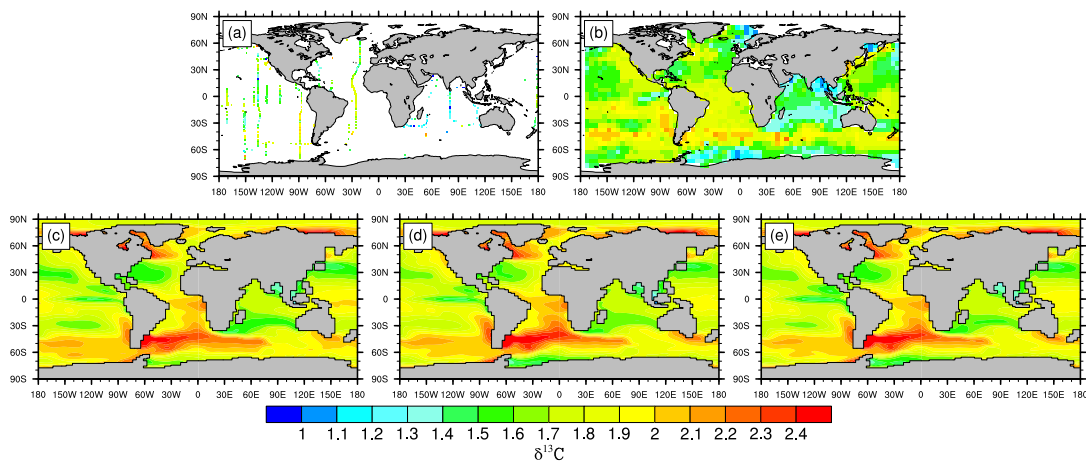


**Fig. 6.** Surface values of  $\delta^{13}\text{C}$  for the 1990s from (a) cruise data compiled by Schmittner et al. (2013), (b)  $5^\circ$  extrapolated gridded data from Gruber and Keeling (1999) and Gruber and Keeling (2001), and (c–e) the biotic model, using the biological fractionation from (c) Rau et al. (1989), (d) Laws et al. (1995), and (e) Keller and Morel (1999).

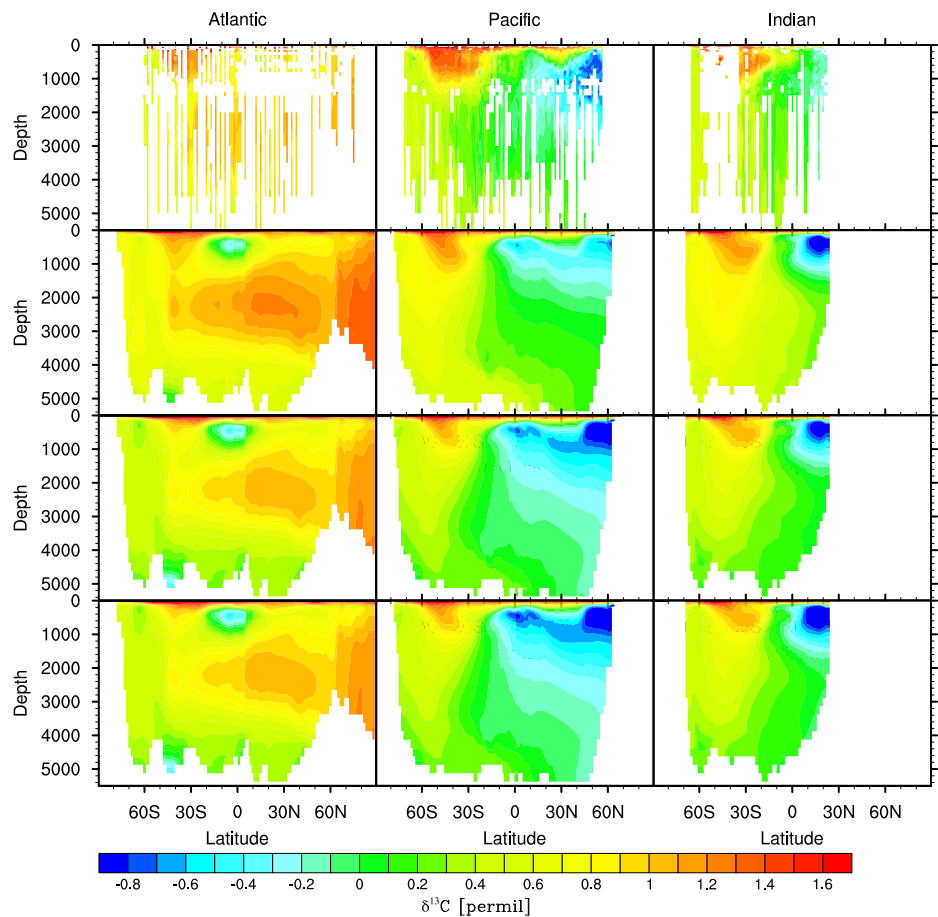


**Fig. 7.** Zonal ocean basin composites from the cruises data compiled by Schmittner et al. (2013) (top row), compared to 1990s zonal basin averages from the model simulation using the biological fractionation from Rau et al. (1989) (second row), Laws et al. (1995) (third row), and Keller and Morel (1999) (bottom row).

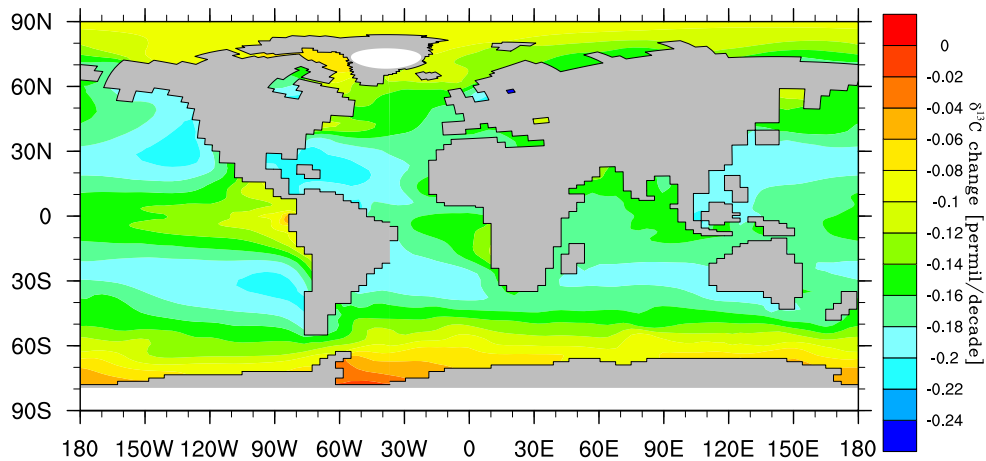


**Fig. 8.** Surface ocean Suess effect (the change in  $\delta^{13}\text{C}$ ) between 1970 and 1990, in  $\text{‰ decade}^{-1}$ .